Chapter 3

The L63 Model

3.1 Modelling by Analogy

In attempting to further understand the dynamics of the atmosphere, meteorologist Edward Lorenz discovered the existence of chaos in a simple numerical model simulating thermal convection (Lorenz (1963)). The notion of chaos is now ubiquitous across many scientific disciplines and is still highly relevant to the study of nonlinear dynamic systems today. In this chapter the Lorenz attractor, which has been explored in great detail since its inception in 1963, is examined to generate insight into the predictability of the more complex climate system under altered forcings.

In section 3.2 the Lorenz-63 (L63) model is described and the model attractor is illustrated for conventional parameter values. The climate of the L63 model is then determined using estimates of the model's probability distributions for each variable and the results are presented in section 3.3. The section begins with a visual analysis of the model climate distributions followed by a quantitative analysis exploring the ergodic hypothesis. The impact of IC ensemble location, in relation to climate prediction, is addressed in section 3.4 by investigating the rates of convergence for model ensembles originating from different regions of the model attractor state space. In section 3.5, the analysis focuses on the behaviour of the model in response to perturbations in the parameter ρ which can be considered analogous to an external forcing on the climate system. Section 3.6 and section 3.7 present the results of experiments exploring the impact of periodic and nonperiodic fluctuations in ρ respectively, on the model climate distributions. The notions of model resonance and hysteresis are examined in each of these sections. Section 3.8 describes the results of experiments in which trends in ρ are imposed on the L63 model to gain insight regarding climate under climate change. The section examines the behaviour of model climate distributions under transient parameter conditions when subject to both chaotic and non-chaotic regions of the parameter space. Finally, section 3.9 discusses the implications of the results for climate model experimental design and the interpretation of climate model output. Focusing on the fundamental issues of climate predictability for nonlinear chaotic systems, recommendations are made for potential experiments using more complex climate models. The usefulness of the term ‘attractor’ in aiding the conceptual understanding of climate in the context of climate change is also reviewed.

3.2 The L63 Attractor

The L63 attractor was first introduced by Edward Lorenz in his seminal paper, Nonperiodic Deterministic Flow (Lorenz (1963)). The ordinary differential equations (ODEs) used to define the system (equations 3.1 to 3.3) are simplified forms of the equations describing thermal convection in a fluid:

$$\frac{dX}{dt} = \sigma(Y - X) \tag{3.1}$$

$$\frac{dY}{dt} = X(\rho - Z) - Y \tag{3.2}$$

$$\frac{dZ}{dt} = XY - \beta Z \tag{3.3}$$

where σ is the Prandtl number, ρ is the Rayleigh number and β is a geometric factor (Tabor (1989)). By convention, the parameters take the values $\sigma = 10$, $\rho = 28$ and $\beta = \frac{8}{3}$. X, Y and Z denote the variables of the model. Figure 3.1 shows a graphical representation of the three-dimensional attractor determined by a single simulation of the model integrated using a common fourth-order Runge-Kutta (RK) integration scheme[1] with a nondimensional time step, $\tau = 0.001$ Lorenz Time Units (LTUs). The integration method and time step used is important in approximating the climate of the L63 system numerically and is discussed further in section 3.3.5. The trajectory shown in figure 3.1 begins from an initial state near the model's attractor and over time the trajectory evolves ever closer towards the attractor. In order to produce figure 3.1, the model is run for 50 LTUs (equal to 50,000 time steps). The attractor is symmetric about the origin in the X and Y dimensions resulting in a two-lobed structure which has often been likened to "butterfly wings" (e.g. van den Berge et al. (2010)).

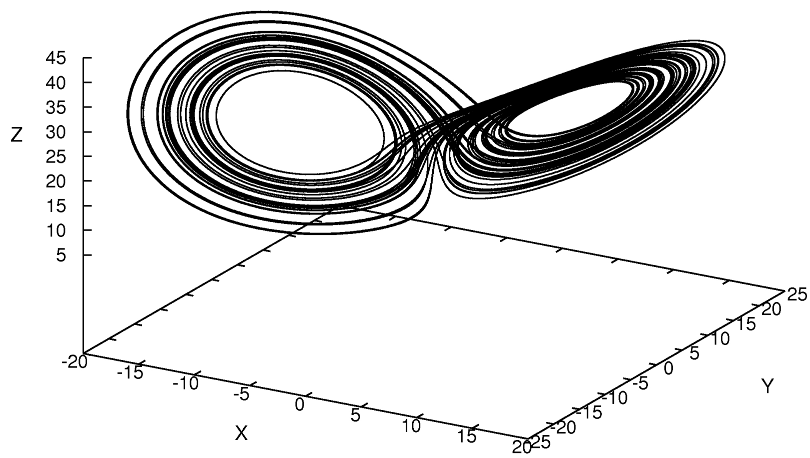

Figure 3.1: Single trajectory for a 50 LTU simulation of the L63 model with ICs $(X, Y, Z) = (1.0, 1.0, 25.0)$.

The L63 model evolves with two characteristic time scales; an oscillation time around the

[1]see http://en.wikipedia.org/wiki/Runge%E2%80%93Kutta_methods

regime centroid, and a residence time within a regime (Palmer (1993)). The oscillation time for a trajectory to orbit one of the lobes on the attractor (also referred to as model regimes in the literature) is typically slightly less than 1 LTU. Figure 3.2 shows the evolution of the model for each variable to illustrate the dynamic behaviour of the model and highlight the nature of the transitions of the trajectories from one regime to the other. The figure is extracted from the same model simulation data as used in figure 3.1 but shown only for the first 20 LTUs of the model run.

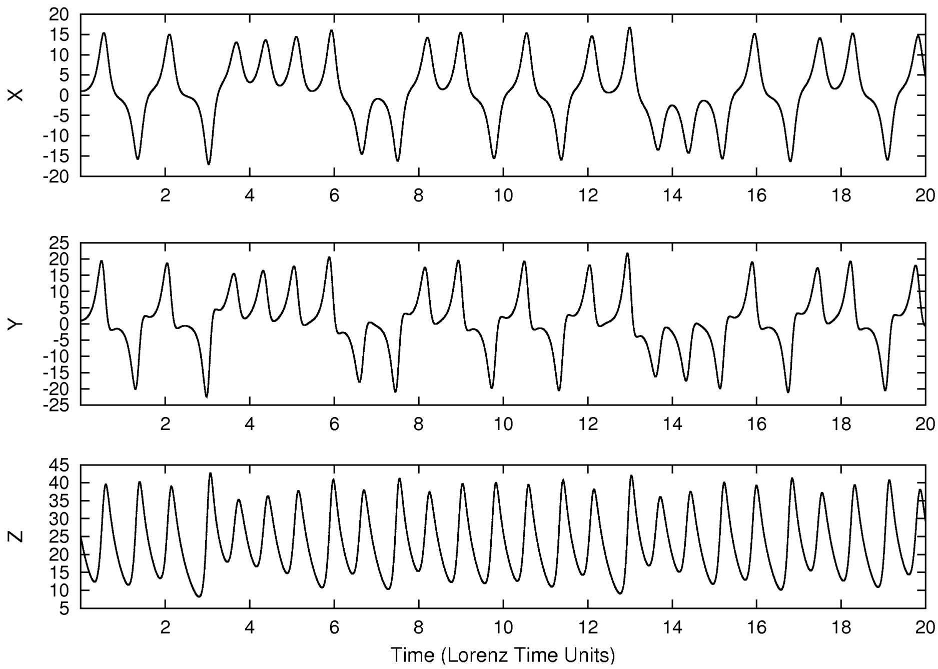

Figure 3.2: Evolution of three model variables for a 20 LTU simulation of a single trajectory from the L63 model, with ICs $(X, Y, Z) = (1.0, 1.0, 25.0)$.

The residence time spent in each of the attractor regimes (evident in the X and Y variables), before a transition to the alternate regime occurs, is variable. In figure 3.2 the trajectory initially transitions after every orbit but at $t = 4$, the trajectory resides in the same regime for four consecutive orbits. The transitions are subject to chaos so a small change in the ICs will ultimately lead to large differences in the evolution of the model trajectories (Lorenz (1963)). The predictability of the deterministic system is therefore limited by uncertainty in the initial state. Nevertheless, it is possible to estimate the likelihood of a trajectory being in a certain region within the model state space. One method to elucidate the likelihood of a trajectory being in a particular region of the model state space is to estimate the probability distributions for each of the three L63 variables for a given choice of parameter values. These distributions provide a measure of climate and represent projections of the possible system states onto each variable of the three-dimensional system. The resultant distributions therefore reveal the 'climate' of the system in relation to the three system variables, X, Y and Z.

3.3 The Climate of L63

To explore the climate of the L63 system, the Perfect Model Scenario (PMS) is adopted. The PMS arises when the model we are using admits the same mathematical structure as the system that generates the observations (Smith (2007)); in other words the system and the model are the same.

3.3.1 Defining the climate of the L63 system

Establishing a single definition of climate for the Earth system is non-trivial (see discussion in section 2.1.1) but the climate of the autonomous L63 model (with fixed parameters) can be well defined. The climate is given by the distribution of states, across all model variables, consistent with the model's attractor. For fixed parameters, the probability of a trajectory being in a particular region of the model state space is constant. For any given variable of the model, the climate is therefore manifest as a probability distribution over the range of possible variable states.

There are at least two methods for numerically estimating the probability distributions (which will hereafter also be referred to as the model climate distributions) for each of the L63 variables. Firstly, a single realisation of the model can be run for a long period of time and a frequency distribution for each model variable produced. If the distributions remain unchanged when running the model for a longer period of time, then the distributions have converged towards the model's climate distributions. Secondly, a large number of IC ensemble members can be run for a fixed length of time and the final states of each member used to generate a frequency distribution. If the length of the model simulation time is sufficient for the trajectories to adequately *explore* the attractor state space then the ensemble distributions will approximate the climate distributions for the model variables. According to the ergodic hypothesis, the distributions from each of the two methods should be equivalent.

To test the ergodic hypothesis for the L63 model, and provide estimates of the model's climate distributions, a number of model runs are performed. Initially, the single trajectory approach to estimating the climate distributions is tested and the length of time required for the frequency distributions to converge is investigated.

3.3.2 Convergence of single trajectory distributions

A single trajectory is initiated at a point close to (but not on) the attractor[2] and over the course of the model simulation, the trajectory moves towards the attractor. The frequency distributions of the model variables are determined for the single model realisation over increasing simulation periods, from 1 LTU to 10,000 LTUs. The frequency distributions for the X variable are given

[2] IC is $(X, Y, Z) = (1.0, 1.0, 25.0)$; a state that visually appears to be near the saddle point of the attractor shown in figure 3.1.

in figure 3.3 (the corresponding distributions for the Y and Z variables are given in Appendix A).

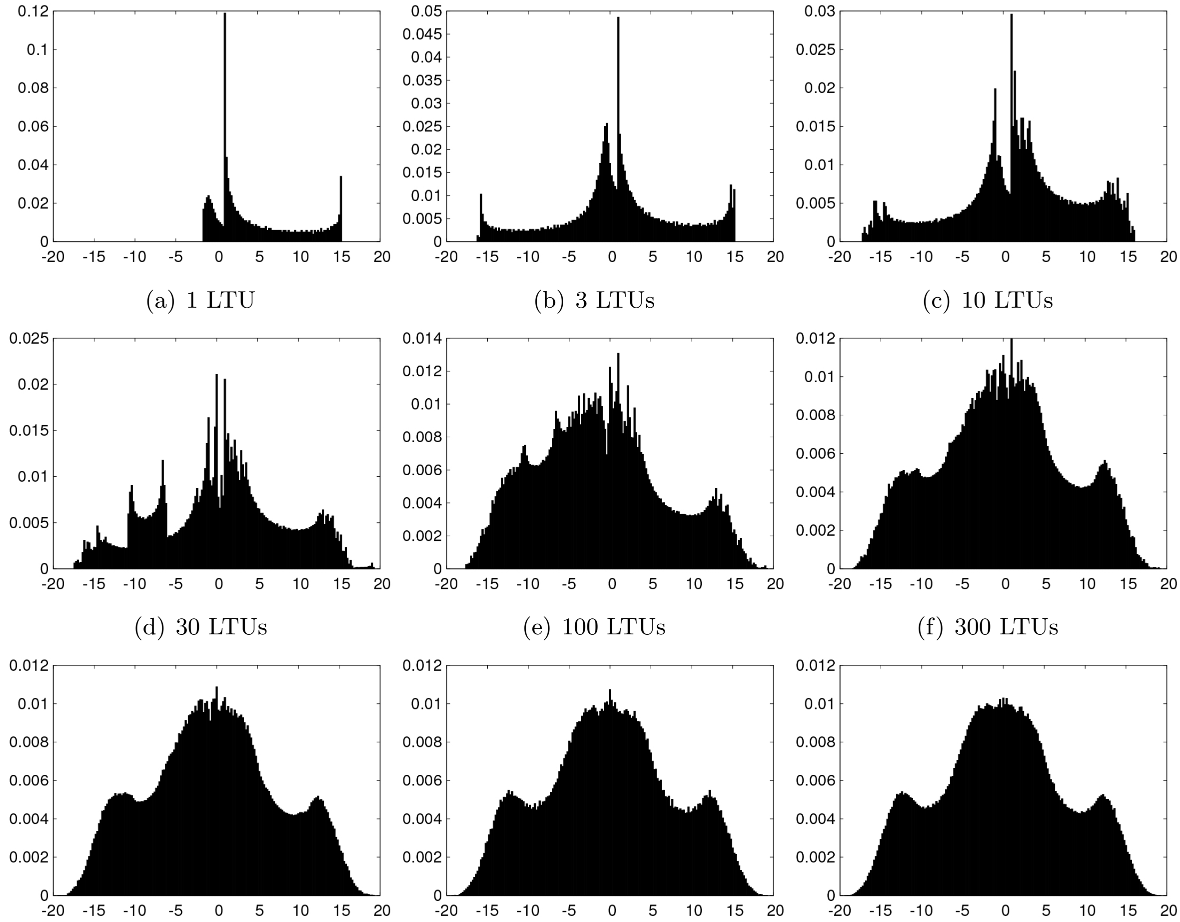

(a) 1 LTU (b) 3 LTUs (c) 10 LTUs

(d) 30 LTUs (e) 100 LTUs (f) 300 LTUs

(g) 1,000 LTUs (h) 3,000 LTUs (i) 10,000 LTUs

Figure 3.3: Normalised frequency distributions of the X variable from a single trajectory of the L63 model with ICs $(X, Y, Z) = (1.0, 1.0, 25.0)$, over increasing time periods. In each plot, the x-axis corresponds to the X variable and the y-axis corresponds to the frequency per occupied bin; bin width $= 0.2$.

The distribution depicted in figure 3.3(a) shows the distribution of model states over the first LTU of the model run. The distribution is highly asymmetrical as the trajectory only has sufficient time to propagate around one of the two model regimes. As the time period increases, the asymmetry becomes less pronounced because the trajectory spends approximately the same amount of time in each of the model regimes. The results illustrated in figure 3.3 show that the model distributions converge over time. The distribution that results after 10,000 LTUs, shown in figure 3.3(i), is a relatively smooth symmetric distribution with a primary peak at the origin and two secondary peaks at $X \approx \pm 13$. The distributions in the Y and Z variables similarly show convergence over time (see figures A-1(a) and A-2(a) in appendix A). In order to demonstrate the ergodicity of the L63 model for conventional parameters, the following sections explore the convergence of IC ensemble distributions and compare the rates of convergence to that observed in the single trajectory distributions.

3.3.3 Convergence of initial condition ensemble distributions

In this section, results from large IC ensemble model runs are presented as an alternative approach to estimating the L63 model's climate distributions. Assuming a knowledge of the range of possible model state values but no prior knowledge of the model's climate distributions, a 100,000 member IC ensemble is selected with ICs that are evenly spaced along a transect from plausible low values, X_l, Y_l, Z_l $(-20, -25, 1)$, to plausible high values, X_h, Y_h, Z_h $(20, 25, 40)$. The ensemble is run for 1,000 LTUs and the distributions are shown at given time instants in the simulation period. The ensemble distributions displayed consist of a single state for each ensemble member. The distributions for the X variable are given in figure 3.4 (the corresponding distributions for the Y and Z variables are given in Appendix A).

In order to demonstrate the existence of ergodicity in the L63 model numerically, the distributions that result using long time interval integrations of a single trajectory, as explored in section 3.3.2, have to be shown to be equivalent to the distributions that result from an IC ensemble. Indeed, the ensemble distribution in figure 3.4(i) for the X variable closely resembles the distribution shown in figure 3.3(i), thus appearing to support the ergodic hypothesis for the L63 model. However, the distributions are not identical. One reason for this might be the size of the ensemble. Whilst a 100,000 member IC ensemble would be considered very large in a climate modelling context, the number of individual data points is two orders of magnitude smaller than the 10,000,000 data points that constitute the distribution given in figure 3.3(i). In addition, a 1,000 LTU integration time step may still be too short to guarantee that the ensemble members have spread around the attractor and can be considered independent of the IC ensemble design; an issue explored in the next section. Because of the chaotic nature of the L63 model and the fact that over time the trajectories move towards the attractor, a longer integration with more ensemble members would better approximate the model's climate distributions.

3.3.4 Time to converge to the model climate

In this section, the rates at which single trajectory distributions and IC ensemble distributions converge to the L63 model climate is presented. At any point in a model simulation a single trajectory may spend an unusually long time in one of the two regimes on the attractor. Consequently, the simulation time required for frequency distributions extracted from a single trajectory to approach the model's underlying climate distributions ought to be longer than the respective simulation time required for an IC ensemble. Given the chaotic nature of the L63 model, ensemble members initiating from different ICs will spread across the attractor independently from one another. Evidence that this occurs in the L63 model is apparent when comparing figure 3.3(e) to figure 3.4(g), both of which show frequency distributions after a 100

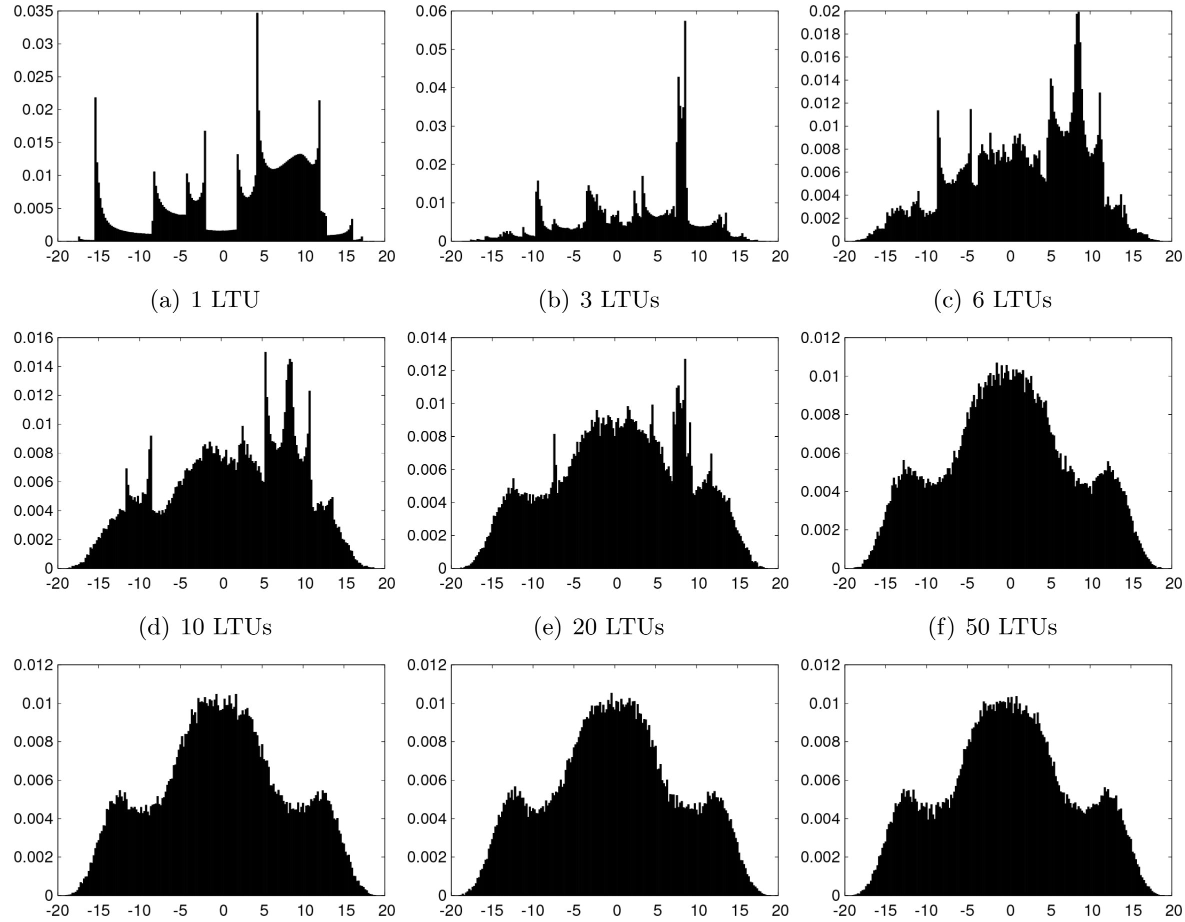

(a) 1 LTU (b) 3 LTUs (c) 6 LTUs

(d) 10 LTUs (e) 20 LTUs (f) 50 LTUs

(g) 100 LTUs (h) 300 LTUs (i) 1,000 LTUs

Figure 3.4: Normalised frequency distributions of the X variable for the L63 model, from a 100,000 member IC ensemble with ICs spread evenly along a transect from $(X_l, Y_l, Z_l) = (-20, -25, 1)$ to $(X_h, Y_h, Z_h) = (20, 25, 40)$. The distributions show the states of each ensemble member at the given time instant in the simulation period. In each plot, the x-axis corresponds to the X variable and the y-axis corresponds to the frequency of ensemble members per occupied bin; bin width = 0.2.

LTU run of the L63 model. The distribution from the single trajectory given in figure 3.3(e) is asymmetric and clearly different from the converged distribution that results over a longer simulation period. In figure 3.4(g), the distribution is largely symmetric and visually resembles the converged distribution shown in figure 3.3(i).

The distributions associated with the 100,000 member IC ensemble simulation at 1,000 LTUs (a long time with respect to the characteristic time scales of the system) provides benchmark "equilibrium" climate distributions, to which other distributions may be compared. Ideally, one would create distributions from an even larger ensemble and run the model for an even longer simulation period but practical considerations ensure restrictions. The 'equilibrium' climate distributions for each of the model variables are given in figure 3.5; where figure 3.5(a) is a reproduction of figure 3.4(i).

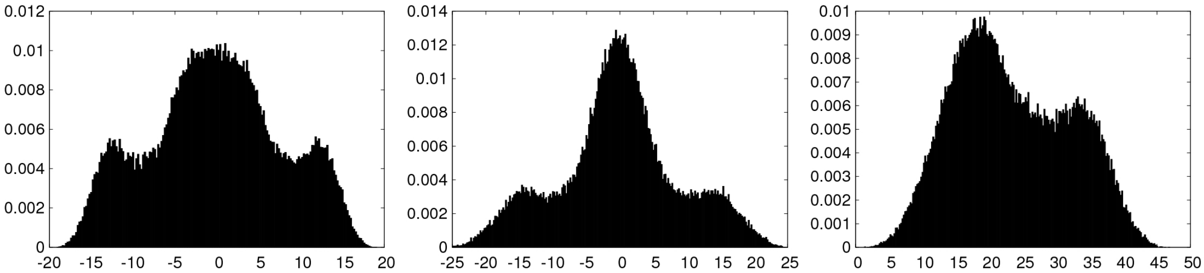

(a) X (b) Y (c) Z

Figure 3.5: Normalised frequency distributions for the three variables of the L63 model, from a 100,000 member IC ensemble with ICs spread evenly along a transect from $(X_l, Y_l, Z_l) = (-20, -25, 1)$ to $(X_h, Y_h, Z_h) = (20, 25, 40)$. The distributions show the states of each ensemble member at the 1,000 LTU time instant in the simulation period. In each plot, the x-axis is given in the panel title and the y-axis corresponds to the frequency of ensemble members per occupied bin; bin width = 0.2.

One method to quantitatively compare distributions is the Kolmogorov-Smirnov (KS) test. The KS statistic, D, is defined as the maximum value of the absolute difference between cumulative distribution functions (Press et al. (1992)). When comparing two cumulative distribution functions, $S_{N_1}(x)$ and $S_{N_2}(x)$, the KS statistic is given by equation 3.4:

$$D = \max_{x_{min} \leq x \leq x_{max}} \mid S_{N_1}(x) - S_{N_2}(x) \mid \tag{3.4}$$

When $D = 1$, the distributions are entirely different; the ranges of the data from which the distributions are derived do not crossover. As $D \to 0$ the distributions become more similar; when $D = 0$, the distributions are identical. To establish the significance of the test statistic, a critical value of D (K_α) can be determined according to equations 3.5 and 3.6 such that the null hypothesis[3] can be rejected at level α if:

$$\sqrt{\frac{nn'}{n+n'}} D_{n,n'} > K_\alpha. \tag{3.5}$$

$$Pr(D_{n,n'} \leq K_\alpha) = 1 - \alpha \tag{3.6}$$

where n and n' are the sample sizes of the two distributions. In a number of subsequent comparisons shown in this thesis, the KS statistic compares two ensemble distributions with 10,000 members each; when $n = 10000$ and $n' = 10000$, the critical KS value at the 95% confidence level is $K_\alpha = 0.019$. Whilst the significance of the D values presented in this chapter and the following chapters can therefore be easily obtained, the purpose of using this statistical measure is not to conclusively prove (or disprove) hypotheses at a given level of statistical significance. Rather the KS test is used to provide a simple quantitative measure with which distributions can be compared and the interest in this section, and subsequent sections, is predominantly in the *rate* of convergence between ensembles. The measure tends

[3]The null hypothesis asserts that the sample distributions come from the same population

to be more sensitive near the centre of the distribution (where the density is greater) than at the tails (NIST/SEMATECH (2008)) and in this analysis, it is clearly stated when results are impacted by this property. In addition, the KS test makes no assumptions about the shape of the distributions being compared (Gaussian, log-normal etc.) so it is therefore an appropriate measure to use in this study where the distributions are often irregular.

Using the KS test, the equilibrium distributions given in figure 3.5 are compared to the distributions resulting from both the single trajectory method (described in section 3.3.2) and the IC ensemble method (described in section 3.3.3). The distributions used are extracted from the same model runs that generated figures 3.3 and 3.4. The corresponding KS plots, for a period of 300 LTUs, are shown in figure 3.6.

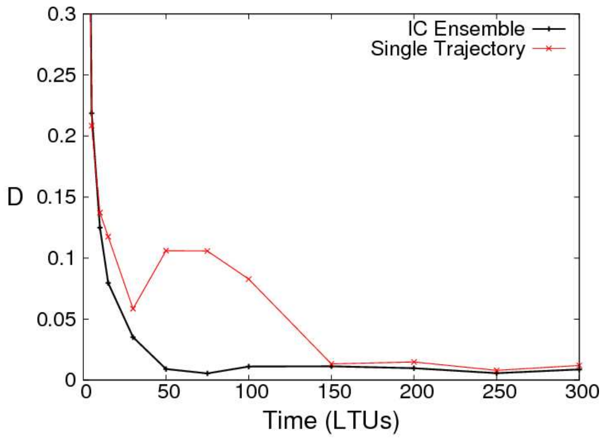

(a) X

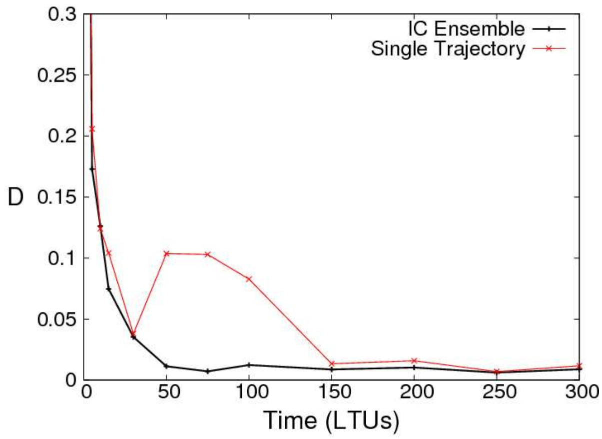

(b) Y

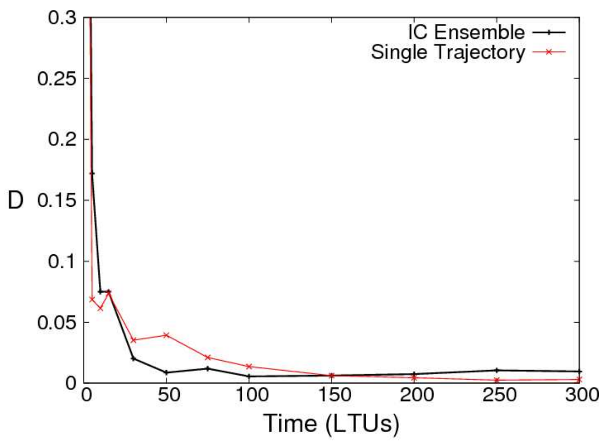

(c) Z

Figure 3.6: KS results showing the comparisons between the equilibrium climate distributions (given in figure 3.5) and the distributions from single trajectory distributions and IC ensembles for each of the L63 model variables under fixed (conventional) parameter conditions.

The ensemble distributions converge towards the climate of the L63 model more rapidly than the single trajectory distributions. After 50 LTUs, the ensemble distributions appear to have converged towards the climate distributions given in figure 3.5. The single trajectory method requires an additional 100 LTUs before the distributions display convergence towards the model climate distributions. The convergence is also less smooth using the single trajectory method because of the chaotic nature of the model which can lead to unusually long residence times within a particular regime. For example, at $t = 30$, D appears to be moving towards zero but at $t = 50$, D has increased. The convergence is faster in the Z dimension for both methods because the two attractor lobes (regimes) occupy broadly the same range in Z whilst the ranges in X and Y are limited to either positive or negative values for a single orbit around a model lobe.

One might question the value in running large IC ensembles which can consume a longer amount of computational time to arrive at the model climate distributions when compared to the single trajectory method. If the model in question is transitive[4] and the parameters of the model are fixed, the case for running large IC ensembles to fully explore the climate distributions may be weak given the additional computational capacity needed to run large IC ensembles. However, it is unknown whether the climate system is transitive, intransitive or almost-intransitive (McGuffie and Henderson-Sellers (2005)) and in the context of climate change, the system parameters (forcings) are certainly changing. This element is explored further in section 3.8 and considered again in later chapters with the insight from additional simple 'climate-like' models. However, there are other potential benefits of running IC ensembles as opposed to single realisations for nonlinear dynamic models and one such reason is outlined in section 3.4, which investigates the 'memory' of the climate system by analogy to the L63 model.

3.3.5 Sensitivity to integration method and time step

In the 1963 paper, Lorenz employs a simple Euler integration method with a time step, $\tau = 0.01$. Whilst sufficient for the model to exhibit chaos and produce a strange attractor, using a simple integration method with a relatively large time step introduces significant temporal truncation errors. Teixeira et al. (2007) investigate the sensitivity of the L63 model's climate to the choice of time step and conclude that the model's climate and model regimes show a complex sensitivity to the time step. The authors therefore suggest that climate statistics derived from climate model output may be affected by truncation errors in the temporal resolution in addition to truncation errors in model spatial resolution. Yao (2005) also examines the sensitivity of the numerical solutions in the L63 model to the time step and states that the numerical truncation errors can substantially alter the shape of the attractor. In order to ensure that the analysis presented in this chapter is robust to the choice of model time step, a number of model versions are run with different time steps for both Euler and RK integration methods.

[4]See glossary definitions.

The Euler Method

For an initial value problem of a given ODE, as expressed in equations 3.7 and 3.8 (where y is an independent variable and t denotes time), one may wish to estimate y at times, $t = t_0, t_1...t_n$.

$$y(t_0) = y_0 \tag{3.7}$$

$$y'(t) = f(t, y(t)) \tag{3.8}$$

Using the Euler method, given in equation 3.9 (where τ is the time step), one computes the tangent to the curve at each time step to approximate the model trajectory.

$$y_{n+1} = y_n + \tau f(t_n, y_n) \tag{3.9}$$

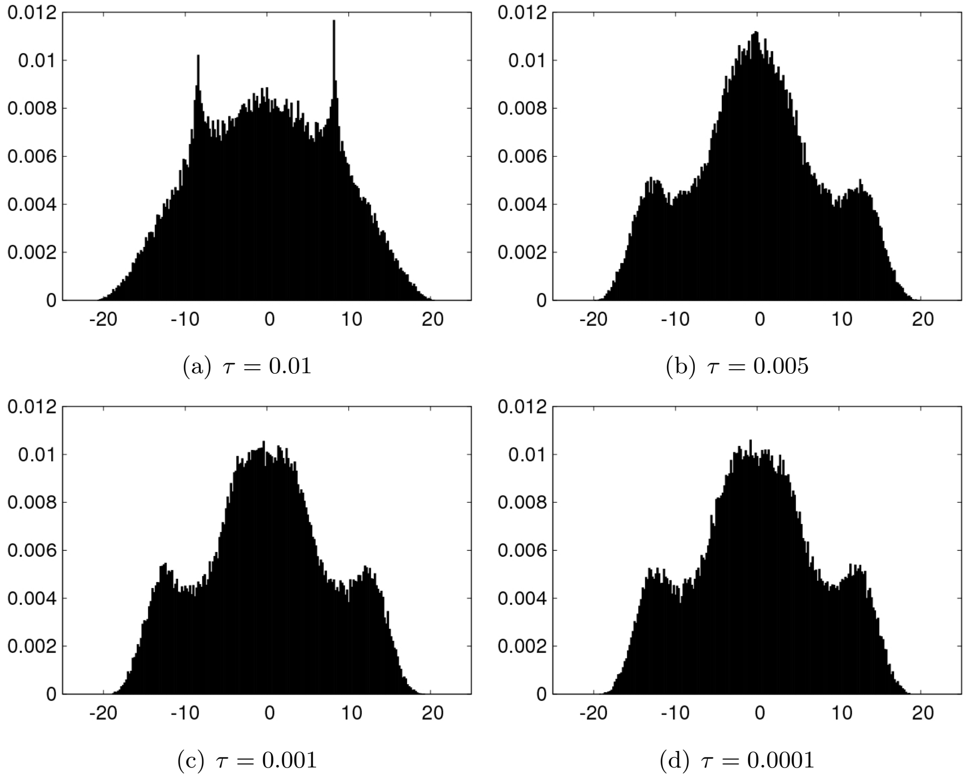

Figure 3.7: Normalised frequency distributions for the X variable in the L63 model from a 100,000 member IC ensemble with ICs taken from the states used to generate figure 3.5. The distributions show the states of the ensemble members after a 100 LTU simulation period using the Euler integration method for given time steps, τ. In each plot, the x-axis corresponds to the X variable and the y-axis corresponds to the frequency of ensemble members per occupied bin; bin width = 0.2.

Figure 3.7 shows the frequency distributions (which approximate the model climate) for the X variable from a 100,000 member IC ensemble when using the Euler integration method for given time steps. Clearly, the time step employed has an impact on the distributions associated with the model attractor. For a time step of $\tau = 0.01$, the model displays a distribution with two sharp peaks centred at $X \approx \pm 9$. By halving the time step to $\tau = 0.005$, a very different climate for the model results, showing a distribution which is more similar to the equilibrium climate distribution shown in 3.5(a) with a primary peak centred at $X = 0$ and two secondary peaks at $X \approx \pm 13$. Also, the range of the ensemble distribution is reduced for smaller time steps. Apparent in figure 3.7(a) but not in figures 3.7(b), 3.7(c) or 3.7(d), are a number of trajectories that occur at values of X close to $X = \pm 20$. For smaller time steps, the range in X is decreased. By reducing the time step to $\tau = 0.001$, and then again to $\tau = 0.0001$, it appears that the distributions have converged towards the model climate distributions. The results show that smaller time steps generate more accurate estimates of the model's climate distributions.

The Runge-Kutta Method

A higher order method of integration is the common fourth order RK method, expressed in equations 3.10 and 3.11:

$$y_{n+1} = y_n + \tfrac{1}{6}\tau\left(k_1 + 2k_2 + 2k_3 + k_4\right) \tag{3.10}$$

$$t_{n+1} = t_n + \tau \tag{3.11}$$

where k_1, k_2, k_3 and k_4 are four measures of the tangent to the model trajectory as given by equations 3.12 to 3.15, and τ is the model time step. The method calculates a weighted average for the slope of the curve which produces a more accurate approximation to the real solution than the Euler method.

$$k_1 = f(t_n, y_n) \tag{3.12}$$

$$k_2 = f(t_n + \tfrac{1}{2}\tau, y_n + \tfrac{1}{2}\tau k_1) \tag{3.13}$$

$$k_3 = f(t_n + \tfrac{1}{2}\tau, y_n + \tfrac{1}{2}\tau k_2) \tag{3.14}$$

$$k_4 = f(t_n + \tau, y_n + \tau k_3) \tag{3.15}$$

Figure 3.8 shows the resulting frequency distributions for the X variable, equivalent to figure 3.7, using the RK method. When $\tau = 0.01$ (figure 3.8(a)), the ensemble distribution is not too dissimilar from the equilibrium climate distribution shown in figure 3.5(a) but the primary peak is split into two peaks at $X \approx \pm 4$. Halving the time step (figure 3.8(b)) removes this anomalous feature but there is still an erroneous aspect to the distribution as the plot reveals a flattened primary peak. For $\tau = 0.001$ and $\tau = 0.0001$, the distribution converges towards the model climate distributions.

Both the Euler and RK methods seem to approach the "true" distributions for the model climate but the RK method appears to be less prone to distribution errors at relatively long time steps. For the analysis presented in this chapter, the higher-order RK method is adopted employing a time step, $\tau = 0.001$. As commented on by Teixeira et al. (2007) and Yao (2005), the impact

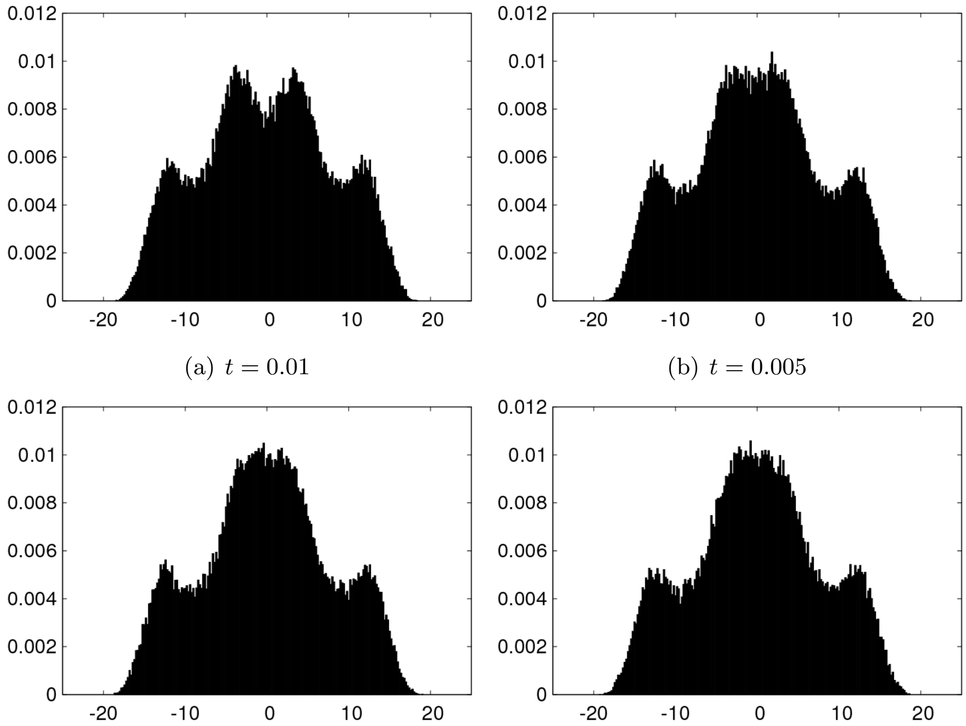

(a) $t = 0.01$

(b) $t = 0.005$

(c) $t = 0.001$

(d) $t = 0.0001$

Figure 3.8: Normalised frequency distributions for the X variable in the L63 model from a 100,000 member IC ensemble with ICs taken from the states used to generate figure 3.5. The distributions show the states of the ensemble members after a 100 LTU simulation period using the Runge-Kutta integration method for given time steps, τ. In each plot, the x-axis corresponds to the X variable and the y-axis corresponds to the frequency of ensemble members per occupied bin; bin width = 0.2.

of temporal truncation error introduced by crude integration methods and time steps is clearly an aspect of climate modelling which needs to be considered more routinely. Whilst the impact may not be seemingly apparent in the results from single realisations, exploring model climate distributions can highlight the sensitivities of particular models to such a class of errors.

3.4 Convergence of Model Ensembles

As discussed in the opening chapters, a primary focus of the research conducted in preparation of this thesis is to further understand the role of IC uncertainty for climate prediction on time scales relevant to climate change adaptation. Determining the time scales over which IC uncertainty is important for the dynamic evolution of the atmosphere-ocean system is therefore of central concern in developing the analogy to the climate system using simple idealised models. The L63 model has been used by a number of authors, in relation to weather forecasting, to develop theory regarding the temporal limits of predictability for single trajectories attributable to IC uncertainty. It has been observed that the deterministic predictability of an individual model trajectory in the L63 model can vary considerably depending on the initial location of the trajectory on the model attractor (Palmer (1993)). The implications of this sensitivity to the location of the initial state on the attractor have been acknowledged in the development of short- and medium-term weather prediction (Palmer (1993), Palmer (1999) and Lea et al. (2000)). However, in this section and in the following sections the L63 model is utilised to extend the analogy in understanding the limits of predictability, attributable to IC uncertainty, for model ensemble "climate" distributions.

In this study, the term *memory* is introduced to refer to the traceability of IC uncertainty in the model climate distributions. On long time scales, relative to the characteristic dynamic time scales of the system, it becomes pertinent to consider whether or not the region of state space in which an IC ensemble originates affects the system's *memory* and thus affects the time scales of predictability for the model climate distributions. The time it takes for IC ensemble distributions, originating in different regions of model state space, to converge provides a measure of the range in the time scales associated with the model memory (for the region of parameter space under investigation). When the ensemble distributions converge to the equilibrium climate distributions (approximated in figure 3.5), the memory of ICs is judged to have been lost.

As the L63 model has been shown to be ergodic (for conventional parameter values) and the model is known to display chaotic behaviour (Lorenz (1963)), the presumption is that ensembles originating from different regions of the model state space would converge to the same distribution and do so at approximately the same rate, thus exhibiting a narrow range in the model memory. Here, the memory of the L63 model is investigated for fixed parameters whilst in section 3.7.5 experiments are conducted to investigate the memory of the L63 model under altered parameter conditions.

Figure 3.9 shows the starting locations of four different 10,000 member IC ensembles superimposed onto the model attractor as depicted in figure 3.1. An ensemble size of 10,000 members is chosen as opposed to 100,000 members (used in earlier plots) in order to decrease the computational time required for model simulations. The locations are chosen from regions spread across the L63 attractor in order to investigate the impact of ensemble location on the

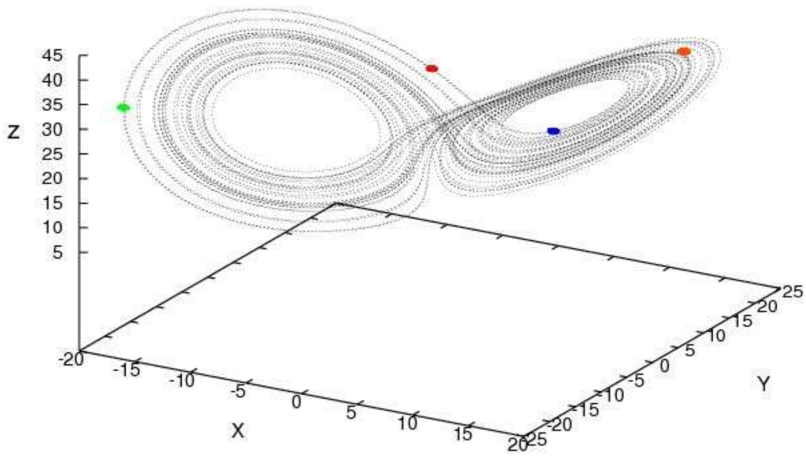

Figure 3.9: Single trajectory from figure 3.1 (dashed line) with four 10,000 member IC ensembles each with members normally distributed about a sphere with diameter, $d = 1$ in each of three dimensions. IC ensembles centred on (from left to right): **1** green points $(-17.228, -22.383, 34.031)$; **2** red points $(-2.520, 5.867, 31.340)$; **3** blue points $(6.683, 9.593, 20.451)$; and **4** orange points $(15.668, 15.564, 36.882)$.

model memory. The ICs within each ensemble are normally distributed within a sphere of diameter, $d = 1.0$. Because of the way the ICs are selected, very few (if any) of the IC states lie precisely on the attractor. However in the analogy to climate prediction, given that the initial state of the climate system is highly uncertain, because of observational uncertainty and sparse data sets, one cannot expect to initiate an ensemble with ICs precisely on any particular climate "attractor".

The four IC ensembles shown in figure 3.9 are run for 100 LTUs and the resulting frequency distributions for each ensemble are compared to the equilibrium climate distributions (shown in figure 3.5) using the KS test as a measure of comparison. The results for each variable are displayed in figure 3.10. The results show that over time the IC ensemble distributions converge towards the equilibrium climate distributions, as expected for a transitive system. After 5 LTUs, there is a large difference between the values of D observed for the different ensembles, with values ranging between $D = 0.21$ (for IC 4 in Y) and $D = 0.58$ (for IC 3 in Z). Over the first 20 LTUs of the model simulation, the values of D decrease rapidly but even after 30 LTUs, the values of D have not reached their minimum, suggesting that the ensemble distributions still retain memory of the ICs. The decrease in D is slower in the Z dimension than in the X and Y dimensions which may be a result of the asymmetry in the distribution and the tendency of the KS statistic to be more sensitive in the high density regions of the distribution (NIST/SEMATECH (2008)). After 40 LTUs in X and Y and 50 LTUs in Z, the KS values converge to a minimum (where $D \to 0$) and the ensemble distributions appear to have converged to the equilibrium climate distributions. Whilst there are differences in the rates of convergence between the IC ensembles, when viewing all three variables together it does not appear that any particular ensemble converges more quickly than the others. The results described here therefore suggest that the memory of ICs in the L63 model is largely

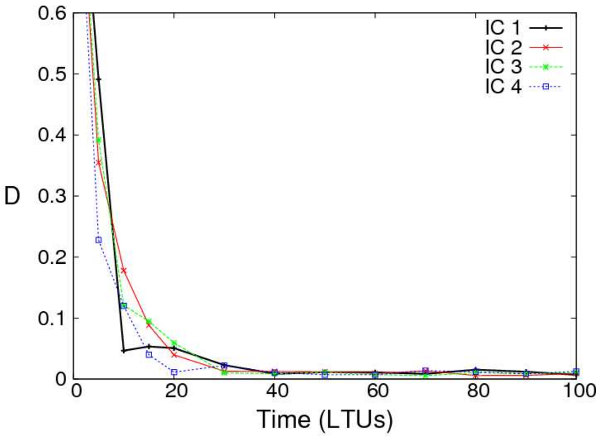

(a) X

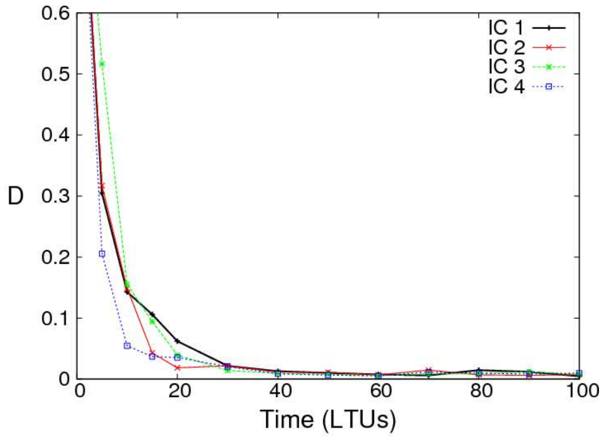

(b) Y

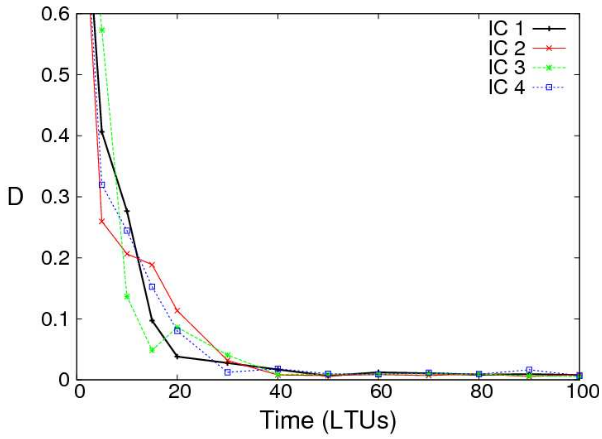

(c) Z

Figure 3.10: KS results showing the comparisons between IC ensemble distributions from IC locations shown in figure 3.9, to the distributions resulting from an IC ensemble with ICs spread proportionally across the attractor for $\rho = 28$, at given time intervals for fixed parameter values.

independent of the initial location of the IC ensemble in the model state space and the memory of ICs is lost on a typical time scale of approximately 40 to 50 LTUs. In section 3.7.5, the impact of nonperiodic variations in ρ on the memory of the L63 model is investigated.

3.5 Varying the Parameter ρ

3.5.1 Motivation for varying ρ

Typically the nonlinear dynamics research community is concerned with *autonomous* dynamical systems whose equations have no explicit dependence on time (Lakshmanan and Rajasekar (2003)). Increasingly however, particularly in relation to climate research, attention is being given to *non-autonomous* dynamical systems whose equations are time-dependent (e.g. Chekroun et al. (2010a)). Unlike global weather prediction models, global climate models are used to determine the evolution of the atmosphere-ocean system under changing boundary conditions and altered radiative forcings. Such changes in the system's forcings are inherently time-dependent and consequently the climate system is a non-autonomous dynamical system. In developing the analogy to the climate system and utilising the notion of a climate attractor, the L63 model is used to explore the impact of climate variability and climate change (i.e. altered forcing conditions) on the probability distributions associated with the model attractor.

Recall that in the L63 system, the forcings are represented by the parameters σ, ρ and β. In the Rayleigh-Benard system, an increase in the temperature difference between the horizontal plates (ρ) leads to an increase in the heat flux (Z). Whilst one must be cautious in using the analogy of the L63 system to the far more complex climate system, the impact of altering ρ can be likened to the impact of changes in the meridional temperature gradient on the equator to pole heat flux (Lea et al. (2000)). More generally, introducing a time-dependence to one of the L63 model parameters can provide useful insight into the possible behaviour of a system's attractor when subject to altered forcings. Consequently, one can loosely relate changes to ρ in the L63 model to changes to the climate forcings in the climate system, such as the impact of GHG concentrations on the radiative forcing of the climate. By exploring the behaviour of a low-order model, when subject to time-dependent parameter changes, insight might be gained about how a more complex nonlinear dynamic system responds. Furthermore, analysis of simple models can help in establishing a theoretical framework to underpin the design of experiments to explore the sensitivity of model climate distributions to scenarios in which the forcing parameters are changing.

3.5.2 L63 attractor for alternative values of ρ

Before imposing a time-varying component in ρ, it is considered necessary to investigate the properties of the L63 model for alternative fixed values of ρ. Rothmayer and Black (1993) provide a concise explanation of the impact of different values of ρ on the model's attractor. When $\rho < 1$, all trajectories propagate towards the origin $(0, 0, 0)$ which is globally attracting. For $\rho \geq 1$ the origin becomes unstable and two new stable fixed points emerge at values $C^{\pm} = (\pm\sqrt{\beta(\rho - 1)}, \pm\sqrt{\beta(\rho - 1)}, \rho - 1)$. At the value $\rho = 24.74$, a Hopf bifurcation occurs (denoted by ρ_H). For values of $\rho > \rho_H$, the fixed points located at $C^{\pm}$ become unstable and chaos ensues (Sparrow (1982)). Therefore ensuring the attractor maintains its chaotic nature, a feature which is an inherent part of the climate system, the following analysis focuses on the climate of the L63 model when $\rho > \rho_H$.

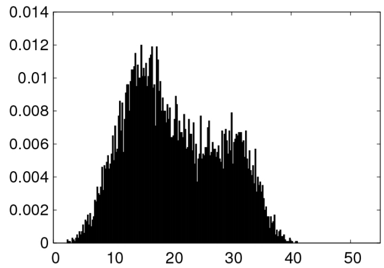

(a) $\rho = 25$

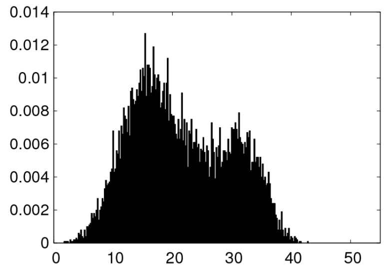

(b) $\rho = 26$

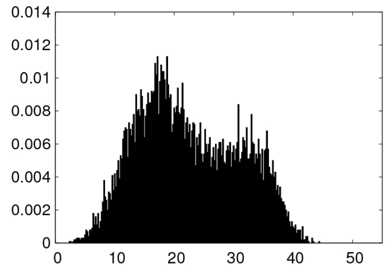

(c) $\rho = 27$

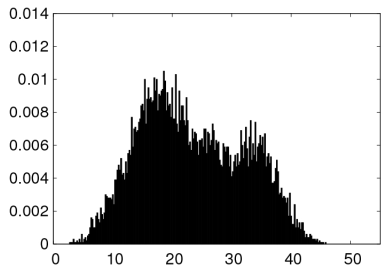

(d) $\rho = 28$

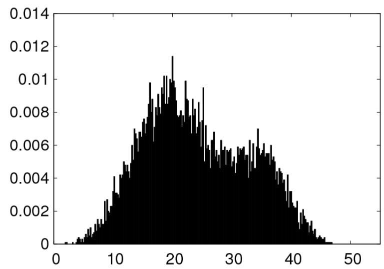

(e) $\rho = 29$

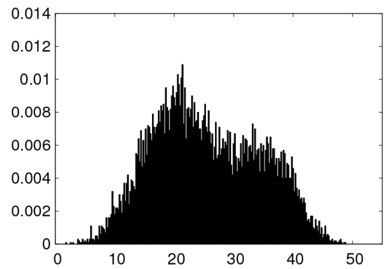

(f) $\rho = 30$

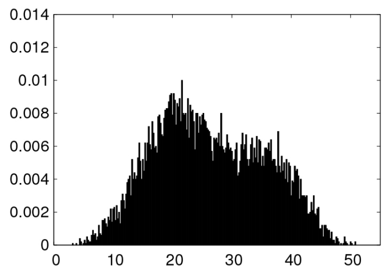

(g) $\rho = 31$

Figure 3.11: Normalised frequency distributions for the Z variable from a 10,000 member IC ensemble after 100 LTUs, for different values of ρ. The IC ensembles are initiated with ICs taken from the first 10,000 members of the equilibrium climate distributions for $\rho = 28$, shown in figure 3.5. In each plot, the x-axis corresponds to the variable Z and the y-axis corresponds to the frequency of ensemble members per occupied bin; bin width = 0.2.

Figure 3.11 shows frequency distributions, from a 10,000 member IC ensemble, for the Z variable after a simulation period of 100 LTUs having evolved with different values of ρ. The Z variable distributions are shown here rather than the X or Y variable distributions (which are shown in figures A-5 and A-6 in Appendix A) because the effect of increasing the parameter ρ on Z forms an interesting analogy to the climate system as described in section 3.5.1. The plots demonstrate that as ρ increases from $\rho = 25$ to $\rho = 31$, the range in the location of the trajectories increases with a notable shift towards higher values of Z. The maximum value of Z increases from $Z_{max} = 41.0$ to $Z_{max} = 50.9$, the mean value increases from $\bar{Z} = 20.5$ to $\bar{Z} = 26.4$ and the minimum value shows relatively little change, moving from $Z_{min} = 2.5$

to $Z_{min} = 3.4$. Consequently, as the parameter ρ increases, the range in Z increases and the peaks become less pronounced (whilst shifting to higher values) but the general shape of the distribution is preserved. The climate of the model is, in a general sense, similar for the range of ρ values chosen whilst the impact of increasing the parameter is most significant in the tails of the distribution. The likelihood of a model trajectory passing through areas of the state space where Z is high is greatly increased for higher values of ρ; the percentage of trajectories above $Z = 40$ increases from 0.04% when $\rho = 25$ to 8.56% when $\rho = 31$. Such a large relative change in the exceedance probabilities at the tails of the distributions, compared to the relative change in the mean, is a common feature of climate model projections (Meehl et al. (2000b)).

The climate distributions for the X and Y variables also remain relatively unchanged for the values of ρ explored here (see figures A-5 and A-6). However, as ρ increases, the number of trajectories moving to the tails of the distributions increases and the range becomes wider whilst maintaining the inherent symmetry about the origin; the maximum/minimum values of X and Y increase/decrease from $X = \pm 17$ and $Y = \pm 22$ when $\rho = 25$ to $X = \pm 20$ and $Y = \pm 28$ when $\rho = 31$. Therefore the signatures of a change in model climate, whilst evident in the shift in the mean for the Z variable, are most prevalent at the tails of the distributions in all model variables.

3.6 Periodic Fluctuations in ρ

The climate system is subject to modes of variability on a number of temporal and spatial scales (Ghil (2002)). Such variability can sometimes be attributed to fluctuations in the forcings on the climate system (Petit et al. (1999), Rind (2002)). In order to examine the potential influence of continuously varying forcings on the climate, using the analogous behaviour of the L63 model, a number of experiments are conducted in which the L63 model is subject to smoothly varying fluctuations in ρ. Adopting the range of ρ values explored in section 3.5.2, perturbations are added to a reference value, ρ_0, in the form of a sinusoidal time series according to the equation:

$$\rho(t) = \rho_0 + A(\sin 2\pi f t) \tag{3.16}$$

where A is the wave amplitude, t represents time and f denotes a controlling factor to adjust the frequency of the wave (with units LTU^{-1}); when $f = 1$ the wavelength is 1 LTU.

To investigate the impact of a non-stationary ρ parameter, a range of f values between $0.1 < f < 10$ are selected and ρ_0 is set to $\rho_0 = 28$ with $A = 3$ so that ρ oscillates between $25 < \rho < 31$. The L63 model is then run with an IC ensemble using initial values from the states of the first 10,000 members of the equilibrium distributions shown in figure 3.5. The resulting distributions for the ensemble simulations are displayed in figure 3.12 at 40 LTUs into the model simulation, as a 40 LTU time scale has been determined broadly sufficient to allow the ensembles to converge to the model climate distributions (see section 3.4).

When the model is subject to a stationary value of ρ, unsurprisingly the ensemble distributions do not change and the plots shown in figures 3.12(b) to 3.12(d) are very similar to the equilibrium climate distributions shown in figure 3.5; albeit less smooth because of a reduced number of ensemble members. Similarly, for a low frequency fluctuation in ρ ($f = 0.1$), as illustrated in figure 3.12(e), the ensemble distributions that occur after a simulation period of 40 LTUs are similar to the equilibrium climate distributions. The slow modulations between $\rho = 25$ and $\rho = 31$ lead to a relatively smooth response in the distributions and as seen in the fixed ρ plots given in figure 3.11 (for the Z variable), the distributions do not vary considerably in this parameter space.

However, when $f = 1$ the distributions that occur after a 40 LTU simulation period are very different from the model climate distributions for $\rho = 28$. When $f = 3$, and to a lesser extent when $f = 5$, the distributions are also dissimilar to the model climate distributions. By design, the frequency with which ρ is varying when $f = 1$ is of a similar time scale to the time it takes for a trajectory to orbit one of the attractor regimes. The model trajectories appear to be resonating with the fluctuations in ρ. This apparent resonance leads to dramatic changes in the distributions of the model variables and significantly alters the model climate. Further discussion of the impact of model resonance in the L63 model and its potential significance for climate change prediction is given in section 3.9.2.

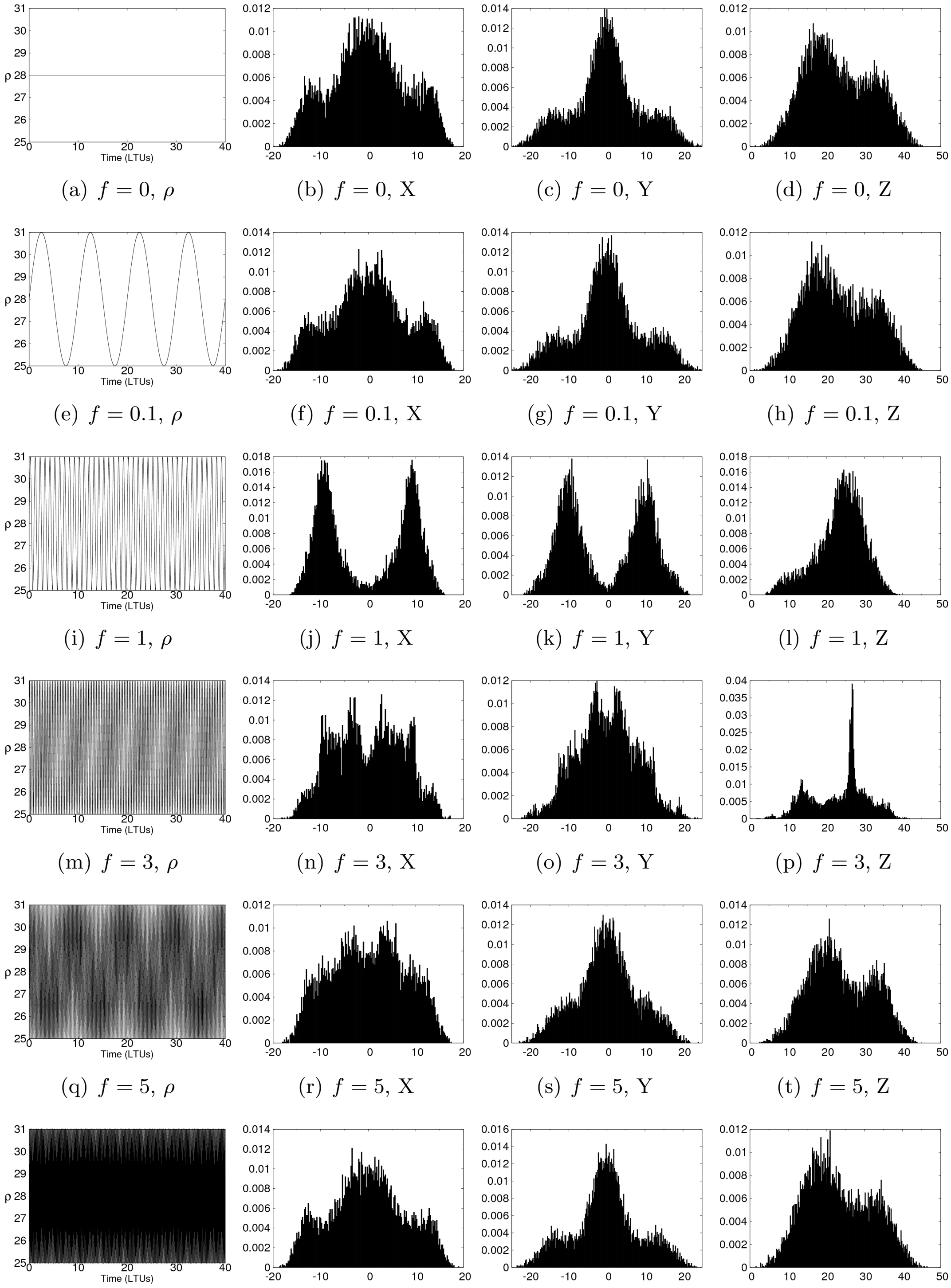

(a) $f = 0$, ρ (b) $f = 0$, X (c) $f = 0$, Y (d) $f = 0$, Z

(e) $f = 0.1$, ρ (f) $f = 0.1$, X (g) $f = 0.1$, Y (h) $f = 0.1$, Z

(i) $f = 1$, ρ (j) $f = 1$, X (k) $f = 1$, Y (l) $f = 1$, Z

(m) $f = 3$, ρ (n) $f = 3$, X (o) $f = 3$, Y (p) $f = 3$, Z

(q) $f = 5$, ρ (r) $f = 5$, X (s) $f = 5$, Y (t) $f = 5$, Z

(u) $f = 10$, ρ (v) $f = 10$, X (w) $f = 10$, Y (x) $f = 10$, Z

Figure 3.12: Normalised frequency distributions for a 10,000 member IC ensemble after a 40 LTU model run for given values of f. ICs are taken from the first 10,000 members of the climate distributions shown in figure 3.5. The left column shows the time series' in ρ, the distributions for X, Y and Z are shown in the centre-left, centre-right and right columns respectively. In the L63 variable plots, the y-axis corresponds to the frequency of ensemble members per occupied bin; bin width = 0.2.

For relatively high frequency fluctuations of $f = 10$, the ensemble distributions shown in figure 3.12(v) to 3.12(x) appear similar to the climate distributions. It is postulated that the rapid perturbations to ρ act as stochastic *noise* in the model and the consequence is that model trajectories evolve in a manner consistent with the model attractor at the mean reference value, $\rho_0 = 28$.

To further elucidate the impact of a sinusoidal variation in the model parameter ρ, the KS test is utilised to reveal the temporal evolution of the ensemble distributions for different values of f, relative to the ensemble climate distributions when ρ is fixed at $\rho = 28$. Figure 3.13 shows the time series' of the KS comparisons for each model variable. The ensembles are all initiated with the same ICs so $D = 0$ at time $t = 0$. The highest values of D are observed when $f = 1$, consistent with the significantly altered distributions shown in figures 3.12(j) to 3.12(l). D is also high when $f = 3$ in the Z variable largely due to a peak in the ensemble distributions at $Z \approx 27$ (see figure 3.12(p)). In the X and Y variables, the lowest KS values are observed when $f = 0.1$ and $f = 10$. When $f = 0.1$, there is an element of periodicity in the X and Y variables but the periodicity is most evident in the Z variable. The periodicity has a wavelength of 5 LTUs which is half the wavelength of the time series in ρ. This is no coincidence and occurs because the model distributions are continuously being altered in response to the changing value of ρ. Every 5 LTUs, ρ returns to $\rho = 28$ and this corresponds to a minimum in the value of D shown in figure 3.13(c). The periodicity in D is most evident in the Z dimension because the response of Z distributions to different values of ρ is larger than in the X and Y dimensions, particularly towards the upper tail of the distributions (as shown in figure 3.11). It is interesting to note that the value of D appears to reach a lower minimum every 10 LTUs (at 10, 20, 30 LTUs etc.), corresponding to the recurrence in $\rho = 28$ on the positive gradient of the sinusoid. This result demonstrates a memory of the forcing pathway, providing circumstantial evidence of hysteresis in the L63 model.

3.6.1 Implications for ergodicity

The ergodic assumption is shown to be valid for the L63 model under fixed parameter conditions (see section 3.3.3) but in this section, the ergodic assumption is tested when ρ varies periodically. A single realisation of the model is run with $f = 1$. The single trajectory is illustrated in figure 3.14 after a 40 LTU model simulation. Unlike the evolution of the single trajectory under fixed ρ, shown in figure 3.2, when the model is subject to periodic changes in ρ the trajectory evolves with some orbits passing much closer towards the centre of the two attractor lobes identified in section 3.2. The orbits also lose an element of regularity; in figure 3.2 the orbits are largely concentric (away from the saddle point) but in figure 3.14 the concentric behaviour is no longer observed.

In order to test the ergodic assumption, frequency distributions from the single model trajectory are compared to the IC ensemble distributions described in section 3.6. Because the value of ρ is varying in time, it is necessary to determine the ensemble distributions over an entire cycle

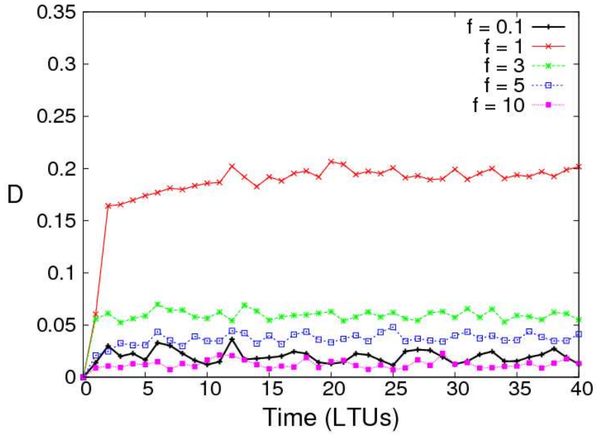

(a) X

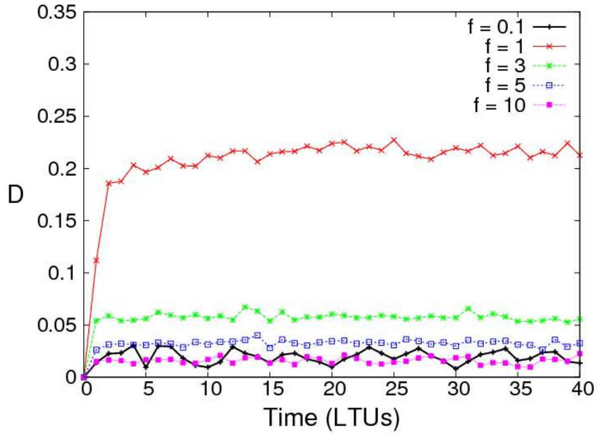

(b) Y

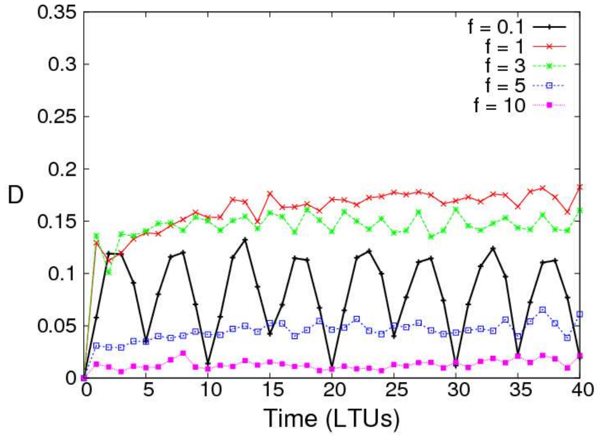

(c) Z

Figure 3.13: KS results showing comparisons between the ensemble distributions when $f = 0$ (such that ρ is fixed at $\rho = 28$) and the ensemble distributions for other values of f for each of the L63 model variables subject to periodic variations in ρ.

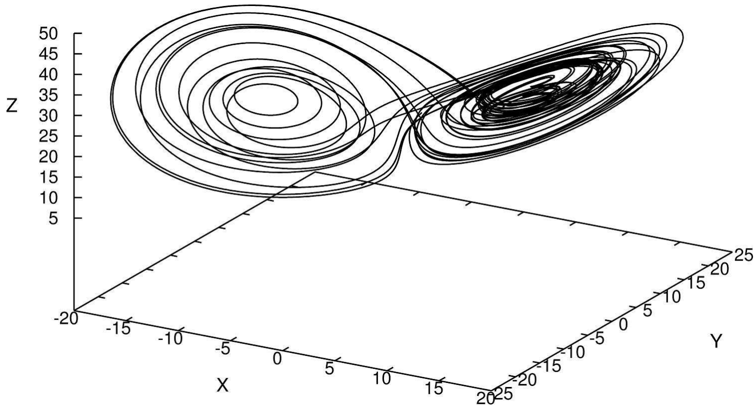

Figure 3.14: Evolution of model "attractor" for a 40 LTU simulation of a single trajectory from the L63 model with $f = 1$ and ICs $(X, Y, Z) = (2.12, -0.72, 25.08)$.

in ρ rather than a specific instant in time. A cycle in ρ is equivalent to 1 LTU when $f = 1$ (see figure 3.12(i)). The time step used in the model simulations is $\tau = 0.001$ so extracting 10,000 ensemble states at each time step over an interval of 1 LTU means that the ensemble variable distributions consist of 10 million values $(10,000/0.001)$. The ensemble distributions are extracted for the last whole ρ cycle in the 40 LTU model simulation used to construct figure 3.12; from 39 to 40 LTUs. To produce equivalent variable distributions from a single trajectory, the model is run over 10,000 LTUs and states are extracted at each time step so the single trajectory plots also consist of 10 million values. The resulting single trajectory and IC ensemble distributions are shown in figure 3.15.

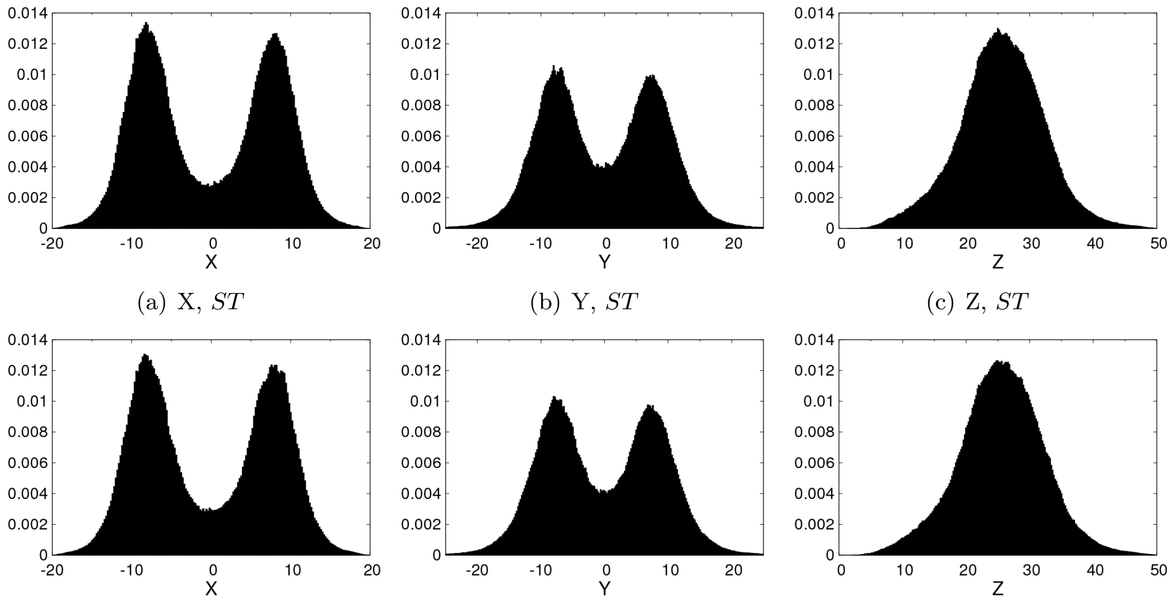

(a) X, *ST* (b) Y, *ST* (c) Z, *ST*

(d) X, *Ens* (e) Y, *Ens* (f) Z, *Ens*

Figure 3.15: Normalised frequency distributions for the L63 model when $f = 1$. Panels (a) to (c) correspond to single trajectory distributions (*ST*) for a 10,000 LTU model simulation and panels (d) to (f) correspond to IC ensemble distributions (*Ens*) extracted from all time steps in the last LTU of a 40 LTU model simulation (with ICs taken from the model states of the equilibrium climate distributions shown in figure 3.5). In each plot, the y-axis corresponds to the frequency of ensemble members per occupied bin; bin width = 0.2.

The distributions in figure 3.15 show that a single trajectory over 10,000 LTUs approximates the same model climate as a 10,000 member IC ensemble over 1 LTU. Therefore the introduction of a smooth (sinusoidal) time-varying parameter (ρ), which induces model resonance, does not mean that the ergodic assumption is invalid. The KS statistics which provide a quantitative comparison of the respective variable distributions are given in table 3.1. All values are very close to $D = 0$ indicating the strength of the similarities in the distributions. However, the value of D for the Z variable comparison is almost double the values of D deduced for X and Y. This is possibly attributable to the unimodal nature of the distribution in Z accentuating the differences in the high density areas towards the centre of the distribution. In the next section, the ergodic hypothesis is examined when the variations in ρ are no longer smooth in time but are nonperiodic and non-repeating.

	X	Y	Z
D	2.72×10^{-03}	2.76×10^{-03}	5.24×10^{-03}

Table 3.1: KS comparison values between single trajectory distributions and IC ensemble distributions shown in figure 3.15.

3.7 Nonperiodic Fluctuations in ρ

3.7.1 Creating a nonperiodic time series in ρ

As described in section 3.5.2 the climate distributions do not vary considerably for fixed values of ρ between $\rho = 25$ and $\rho = 31$. When the model is subject to smooth fluctuations in ρ, as examined in section 3.6, the model displays very different behaviour. The climate distributions are highly sensitive to the frequency of the fluctuations in the parameter ρ and the model exhibits resonance at wave frequencies in phase with the orbiting time scale for model trajectories. Yet for smooth variations in ρ, the application of the ergodic assumption is valid, as shown in section 3.6.1.

In the climate system, there are multiple internal and external forcings which exert an influence on the dynamic evolution of the climate system. External factors which alter the radiative forcings on the climate system, such as solar variability, volcanic eruptions and anthropogenic emissions of GHGs, have differing degrees of periodicity. The cumulative effects of these individual components will likely lead to a highly aperiodic forcing time series on the climate system. In extending the analogy to the climate system, it therefore becomes interesting to consider how the L63 model behaves when subject to irregular fluctuations in ρ.

In order to investigate the impact of irregular fluctuations on the climate distributions of the L63 model, three sine waves of different frequencies are added together to create a nonperiodic time series $\psi(t)$, as shown in equation 3.17:

$$\psi(t) = A\Big(\frac{1}{3}\sin(2\pi)f_i t + \frac{1}{3}\sin(\sqrt{3})f_i t + \frac{1}{3}\sin(\sqrt{17})f_i t\Big) \tag{3.17}$$

$$\rho(t) = \rho_0 + \psi(t) \tag{3.18}$$

where A and t assume the definitions used in equation 3.16 and f_i is a controlling factor to simultaneously adjust the frequencies of the three component waves (with units LTU^{-1}). The three frequency multipliers are chosen as 2π, $\sqrt{3}$ and $\sqrt{17}$ so that the wave is both nonperiodic and also non-repeating on long time scale integrations, relative to the time scales being considered. $\psi(t)$ is added to ρ_0, which denotes the reference (mean) value of ρ, as shown in equation 3.18.

Figure 3.16 shows the time series of ρ over 20 LTUs, when $A = 3$ and $f_i = 1$. The time series is clearly aperiodic and the fluctuations, although entirely deterministic, appear random. The first of the three component sinusoid waves has a frequency exactly the same as the sine wave used in section 3.6 but the second and third component sine waves have slower frequencies ($\sqrt{3}$ and $\sqrt{17}$) which are approximately 3.6 and 1.5 times slower respectively. Therefore, the average wavelength of the combined wave is increased and the results for different values of f_i do not exactly correspond to different values of f explored in section 3.6.

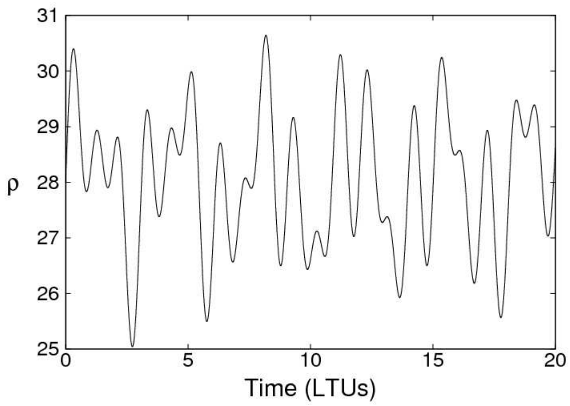

Figure 3.16: Time series of fluctuations in ρ over 20 LTUs; $A = 3$, $f_i = 1$ according to equation 3.18.

3.7.2 IC ensemble results

Model experiments are run over a 40 LTU simulation period with 10,000 member IC ensembles (ICs same as used in figure 3.12). The frequency distributions for each model variable for different values of f_i are given in figure 3.17. The plots are displayed using the same format as that used in figure 3.12. The time series' of ρ over the 40 LTUs of the model simulation, shown in the left column, demonstrate the irregular nature of the parameter fluctuations for different value of f_i because of the irregular nature of the parameter time series'. The corresponding frequency distribution plots illustrate the impact of the parameter fluctuations on the climate distributions of the L63 model for the three model variables after a 40 LTU simulation. It is important to note that the value of ρ is different after 40 LTUs for each different value of f_i. Therefore, in the comparison to the equilibrium climate distributions for $\rho = 28$, one would not expect the distributions to be exactly the same at the 40 LTU time instant; the larger the departure from $\rho = 28$, the greater the difference ought to be. Figure 3.17 doesn't include the distributions when $f_i = 0$ as they are identical to the equilibrium climate distributions given in figures 3.12(b) to 3.12(d).

The fluctuations in ρ clearly affects the climate distributions of the model when varying at intermediate frequencies. When the fluctuations are relatively slow, as demonstrated in figures 3.17(b) to 3.17(d) (where $f_i = 0.1$), the frequency distributions closely resemble the equilibrium climate distributions shown in figures 3.12(b) to 3.12(d). It is important to note that at 40 LTUs ρ approaches the reference value $\rho_0 = 28$ for $f_i = 0.1$. The distributions would be less similar to the fixed $\rho = 28$ climate distributions if observed after 28 LTUs where $\rho \approx 25$. Further analysis to quantify the differences between distributions over time is presented later in section 3.7.3 using the KS test. When the fluctuations are relatively fast, as shown in figures 3.17(v) to 3.17(x), the climate distributions remain largely unchanged. This result is consistent with the outcome observed for fast periodic fluctuations in ρ, shown in section 3.6, where the ρ perturbations are believed to act simply as noise about ρ_0. When the time scale of the parameter fluctuations approaches the orbiting time scale of the L63 model trajectories about the attractor lobes, the distributions become very different to the equilibrium distributions. The differences

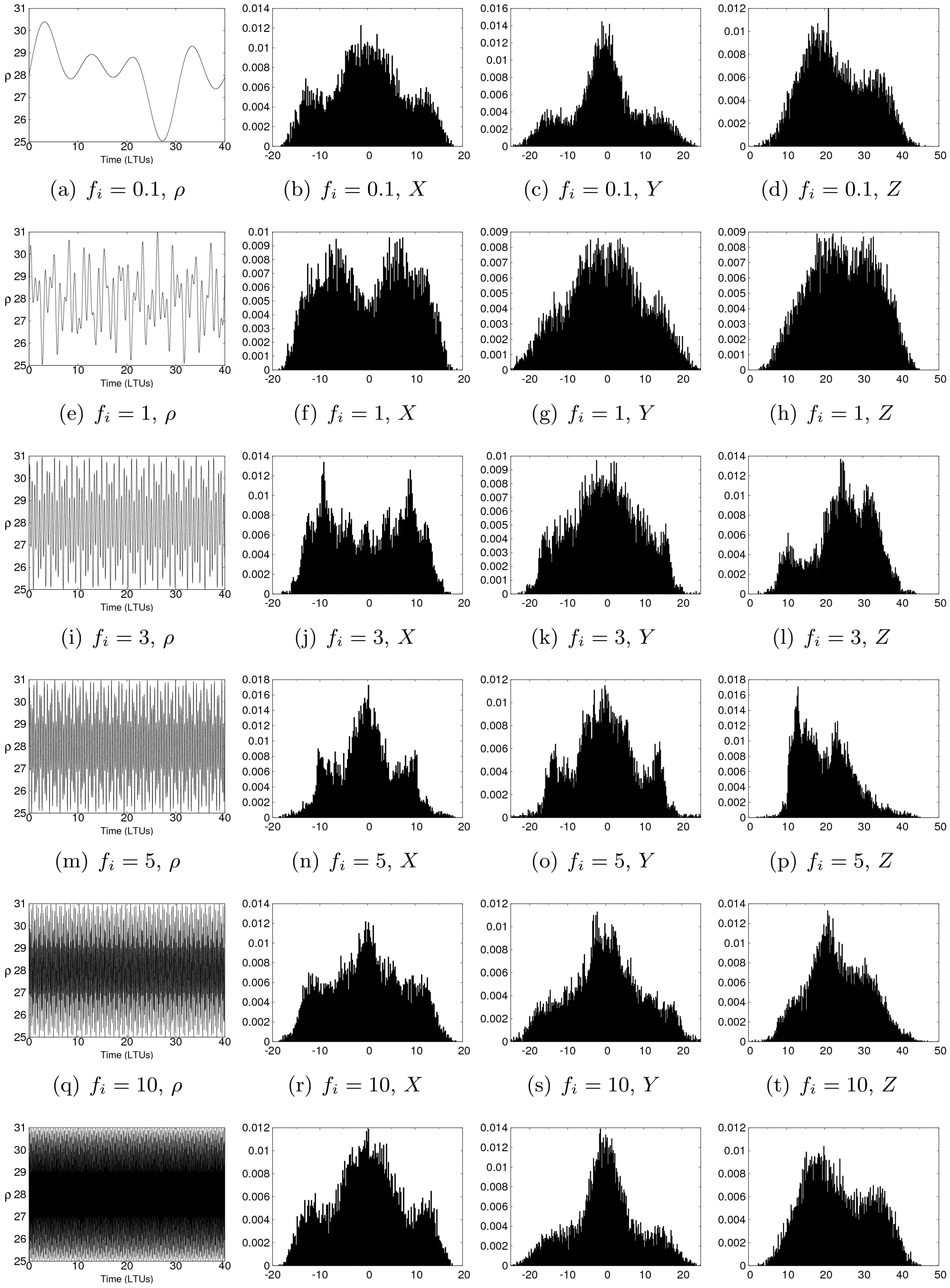

(a) $f_i = 0.1$, ρ (b) $f_i = 0.1$, X (c) $f_i = 0.1$, Y (d) $f_i = 0.1$, Z

(e) $f_i = 1$, ρ (f) $f_i = 1$, X (g) $f_i = 1$, Y (h) $f_i = 1$, Z

(i) $f_i = 3$, ρ (j) $f_i = 3$, X (k) $f_i = 3$, Y (l) $f_i = 3$, Z

(m) $f_i = 5$, ρ (n) $f_i = 5$, X (o) $f_i = 5$, Y (p) $f_i = 5$, Z

(q) $f_i = 10$, ρ (r) $f_i = 10$, X (s) $f_i = 10$, Y (t) $f_i = 10$, Z

(u) $f_i = 30$, ρ (v) $f_i = 30$, X (w) $f_i = 30$, Y (x) $f_i = 30$, Z

Figure 3.17: Normalised frequency distributions for a 10,000 member IC ensemble after a 40 LTU model run for given values of f_i. ICs are taken from the first 10,000 members of the climate distributions shown in figure 3.5. The left column shows the time series' in ρ, the distributions for X, Y and Z are shown in the centre-left, centre-right and right columns respectively. In the L63 variable plots, the y-axis corresponds to the frequency of ensemble members per occupied bin; bin width = 0.2.

in the distributions are apparent in all variables when $f_i = 1, 3$ and 5. Also, unlike in the case where ρ varies periodically in time, the distributions at $f_i = 10$ are noticeably different from the equilibrium climate distributions shown in figures 3.12(b) to 3.12(d). This is caused by the addition of waves with slower frequencies described in section 3.7.1 which act to increase the overall wavelength of the fluctuations in ρ. Consequently, the effect of resonance is observed for higher values of f_i than f which controls the periodic variations in ρ.

3.7.3 KS comparison for nonperiodic variations in ρ

Following the same approach used in section 3.6, the temporal changes in the climate distributions for different values of f_i are determined using a KS comparison to the equilibrium climate distributions for $\rho = 28$. Crucially however, because the time series' in ρ are irregular, choosing to compare the IC ensemble frequency distributions to the equilibrium climate distributions at regular intervals ensures that comparisons occur at time instants when $\rho \neq 28$. Nonetheless, the comparison provides an interesting insight into the behaviour of the ensemble frequency (climate) distributions over time.

Figure 3.18 shows the time series' in the KS statistic (D) over the 40 LTU simulation period for the three model variables. The differences between the distributions are more significant in the Z variable than in the X and Y variable (note the different scale on the y-axis for the Z variable). This is likely to be caused by symmetry in the response of the climate distributions for X and Y which is not present in Z meaning that the shifts in the distribution densities can be accentuated in the Z dimension. For periodic fluctuations in ρ, the highest values of D are observed when $f = 1$ but in the experiments conducted in this section, the highest values of D occur at $f_i = 3$ and $f_i = 5$, consistent with the reasoning that the wavelengths of the nonperiodic fluctuating waves are longer so f and f_i are not exactly equivalent. The differences are also large when $f_i = 1$ and $f_i = 10$ because the distributions are affected by the interaction of waves with different frequencies. One of the most interesting features that emerges from figure 3.18, is the time series in D for the Z variable when $f_i = 0.1$. The time series illustrates that the climate distributions have a strong dependence on the value of ρ. The equivalent time series in ρ is given in figure 3.17(a) and the peaks in D correspond exactly to the peaks and troughs in ρ, with the greatest value of D occurring after 28 LTUs which corresponds to a minimum in the value of ρ.

It appears that resonance is once again a crucial factor in determining the climate distributions of the L63 model under nonperiodic fluctuating parameters. However, with a nonperiodic variation in ρ, it is unclear what the relative contributions of hysteresis and resonance are in the overall distortions to the climate distributions. The interaction of hysteresis and resonance on the L63 model climate distributions is certainly worthy of further investigation. The analysis presented in this thesis only partly addresses this intricate relationship. In the next section, analysis is focussed on exploring the impact of hysteresis in the L63 model. The results are related to the response of the climate system to the precise trajectory of the system forcings.

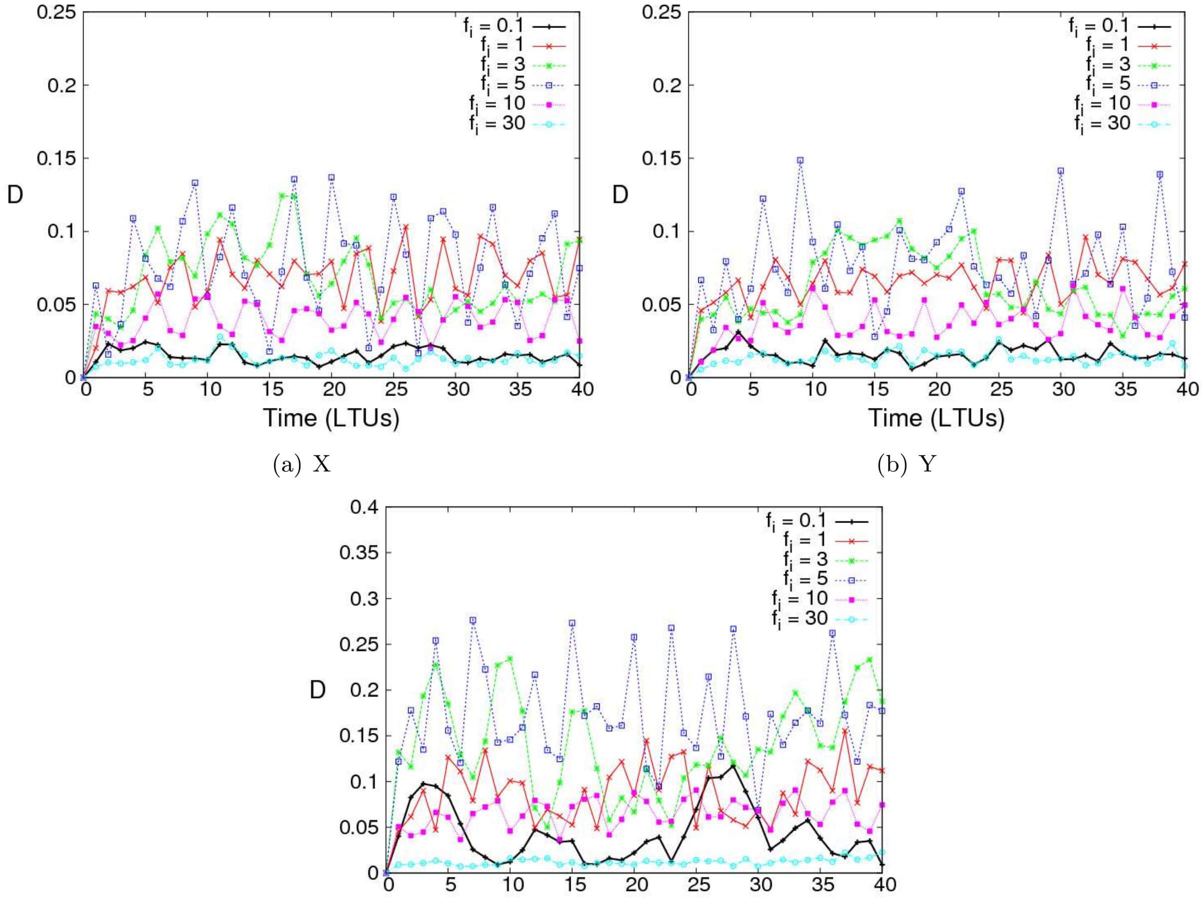

(a) X

(b) Y

(c) Z

Figure 3.18: KS results showing comparisons between the ensemble distributions when $f_i = 0$ (such that ρ is fixed at $\rho = 28$) and the ensemble distributions for other values of f_i for each of the L63 model variables subject to nonperiodic variations in ρ.

3.7.4 Hysteresis in the L63 model with nonperiodic fluctuations in ρ

To examine the extent to which the L63 model exhibits hysteresis (path dependence), the model climate distributions are extracted at time instants when the fluctuating parameter ρ returns to the reference value $\rho = \rho_0 = 28$. As the fluctuations in ρ used in this section are irregular, the instants at which $\rho = \rho_0$ are not evenly spaced throughout the time series'. Using the results of the model run when $f_i = 5$, figure 3.19 shows the distributions in X at specific time instants when $\rho = \rho_0$. Even though $\rho = 28$ at each time instant shown in figure 3.19, the corresponding IC ensemble distributions are clearly very different. In figure 3.19(a), there is a primary peak at the origin but there are defined secondary and tertiary peaks which are not observed in any of the other plots. Figures 3.19(b) and 3.19(d) are both unimodal about the origin but the density is constrained closer to the origin in figure 3.19(d). The distributions in figure 3.19(c) is more uniform across the model state space but there are two peaks located at $X \approx \pm 2$.

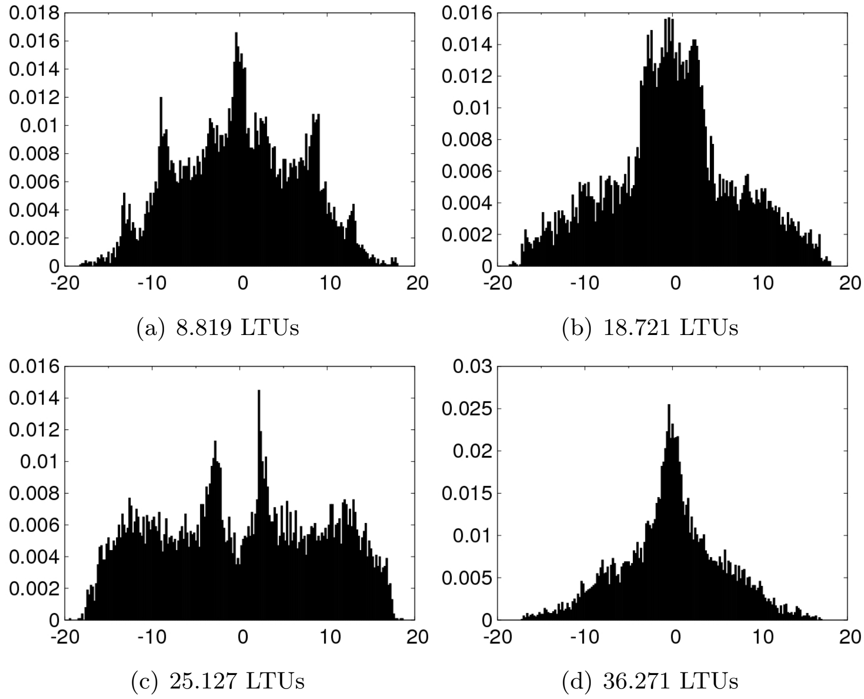

Figure 3.19: Normalised frequency distributions for a 10,000 member IC ensemble at given time instants when $f_i = 5$. In each plot, the x-axis corresponds to the X variable and the y-axis corresponds to the frequency per occupied bin; bin width = 0.2.

The differences in the distributions shown in figure 3.19 imply that the L63 model climate is not only sensitive to the frequency of fluctuations in ρ but also displays hysteresis; the climate distributions are a function of the pathway of ρ. A simple and elegant way to confirm the presence of hysteresis in the L63 model is to invert the time series in ρ when $f_i = 5$ and determine the climate distributions at exactly the same time instants as those illustrated in figure 3.19. If the corresponding distributions are different, then the differences must be attributed to the sensitive dependence of the model to the pathway in the parameter ρ. The time series for ρ in equation 3.18 is inverted (by multiplying $\psi(t)$ by (-1)) and the model ensemble simulation is repeated. Figure 3.20 shows the resulting distributions at the same time instants as those depicted in figure 3.19.

The distributions in figure 3.20 are entirely different to those shown in figure 3.19. Figures 3.20(b) and 3.20(d) no longer display unimodal peaks at the origin but rather show a high density of ensemble members towards the tails of the distributions. Figure 3.20(a) now appears similar to figure 3.19(c) whilst figure 3.20(c) appears similar to figure 3.19(a). The differences confirm the presence of hysteresis in the climate of the L63 model.

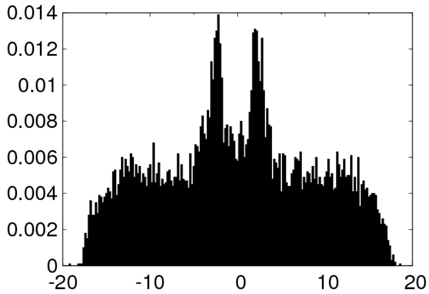

(a) 8.819 LTUs

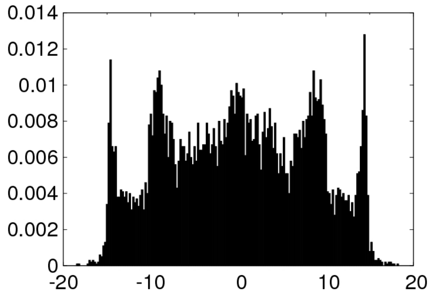

(b) 18.721 LTUs

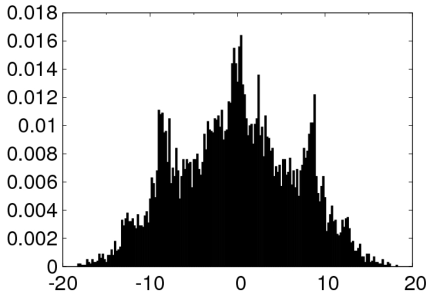

(c) 25.127 LTUs

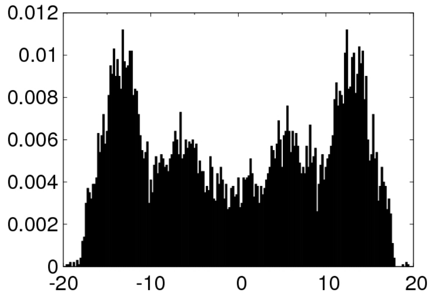

(d) 36.271 LTUs

Figure 3.20: Normalised frequency distributions for a 10,000 member IC ensemble at given time instants when $f_i = 5$ and the time series in ρ is inverted. In each plot, the x-axis corresponds to the X variable and the y-axis corresponds to the frequency per occupied bin; bin width = 0.2.

Implications for ergodicity

The path-dependence of the IC ensemble distributions implies non-ergodic behaviour in this non-autonomous (time-dependent) version of the L63 model; the IC ensemble frequency distributions at an instant in time are different from the frequency distributions over a *long* time interval of a single model trajectory. To confirm this numerically the model configuration used to produce figure 3.19 is run for a single model realisation and the frequency distributions for time intervals centred on the time instants displayed in figure 3.19 are extracted. As the time step $\tau = 0.001$, after 10 LTUs a single trajectory will include 10,000 model states and the distribution of these states can be compared to the ensemble distributions shown in figure 3.19. For example, the first time interval centred on 8.819 LTUs includes the single trajectory states from 3.820 to 13.819 LTUs.

The initial state of the single trajectory is chosen to be the first member of the IC ensemble used to generate figure 3.19: $(X_0, Y_0, Z_0) = (0.62, -0.98, 21.93)$. Figure 3.21 shows four frequency distributions from the single trajectory, subject to nonperiodic fluctuations in ρ at the frequency $f_i = 5LTU^{-1}$, over 10 LTU intervals centred on the time instants considered in figure 3.19. The single trajectory distributions do not resemble the IC ensemble climate distributions at the time instants where $\rho = \rho_0$. The plots show that the ergodic hypothesis is therefore no longer valid for the L63 model when subject to nonperiodic time-dependent fluctuations in the parameter ρ, at least at frequencies which are sensitive to model resonance. Using longer intervals cannot compensate for the differences as the ensemble distributions are time-dependent. The possibility of non-ergodic behaviour in the real climate system as a result of nonperiodic forcing variations has potentially profound implications for climate prediction given the way climate models are currently used to generate future projections. A more detailed discussion of the potential issues for climate prediction is given in section 3.9.

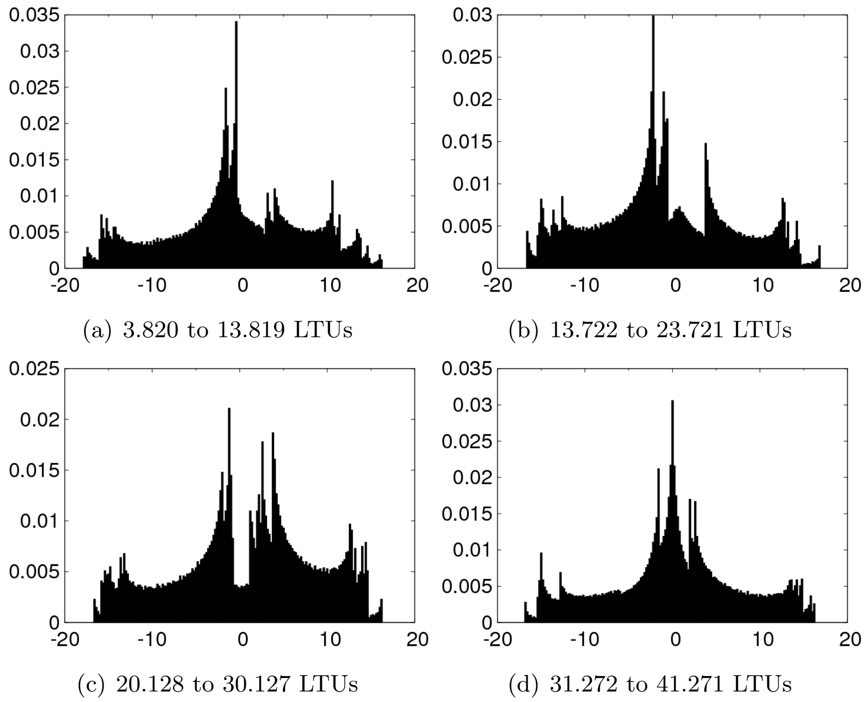

(a) 3.820 to 13.819 LTUs

(b) 13.722 to 23.721 LTUs

(c) 20.128 to 30.127 LTUs

(d) 31.272 to 41.271 LTUs

Figure 3.21: Normalised frequency distributions for a single trajectory with ICs $(X_0, Y_0, Z_0) = (0.62, -0.98, 21.93)$, when $f_i = 5$ over 10 LTU intervals centred on: (a) $t = 8.819$ LTUs; (b) $t = 18.721$ LTUs; (c) $t = 25.127$ LTUs; (d) $t = 36.271$ LTUs. In each plot, the x-axis corresponds to the X variable and the y-axis corresponds to the frequency per occupied bin; bin width = 0.2.

3.7.5 Convergence of model ensembles for nonperiodic forcing in ρ

In section 3.4, it is shown that the IC ensemble location is not important in determining the equilibrium climate distributions for the L63 model with fixed parameters. Additionally, the memory of the model is investigated and shown to exist for a time period of up to approximately 40 LTUs in X and Y and 50 LTUs in Z. It is not obvious however, whether or not IC ensembles from different regions of model state space will converge when ρ is fluctuating periodically or non-periodically. Furthermore, if the ensembles do converge, the rate at which they do so may be different and/or a function of the initial IC ensemble location when subject to fluctuations in the parameter ρ.

The experiment conducted in the previous section, when $f_i = 5$, is used as the reference experiment in this section. Using the same four IC ensembles depicted in figure 3.9, the memory of the L63 model is investigated when subject to nonperiodic fluctuations in ρ. The KS test is once again employed but rather than comparing the distributions from the four ensembles to the equilibrium climate distributions, they are compared to *reference* distributions (which are shown at specific time instants in figure 3.19) resulting from the integration of a 10,000 member IC ensemble, when $f_i = 5$. The IC ensemble has ICs extracted from the first 10,000 members of the 100,000 member equilibrium ensemble distributions illustrated in figure 3.5. The four IC ensemble distributions are compared to the reference distributions at specific time instants over a time period of 100 LTUs and the results are given in figure 3.22.

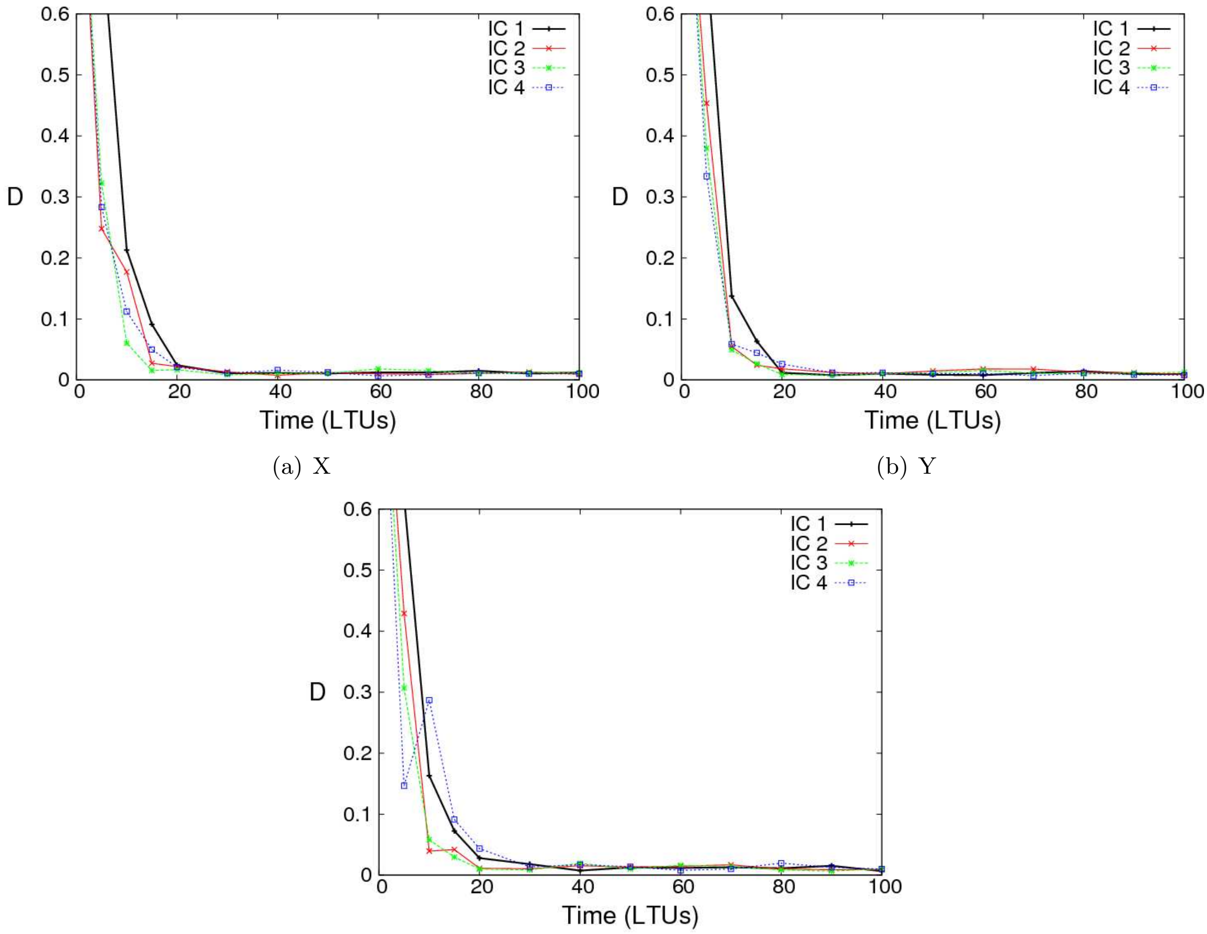

(a) X

(b) Y

(c) Z

Figure 3.22: KS results showing the comparisons between IC ensemble distributions, from IC locations shown in figure 3.9, to the distributions resulting from an IC ensemble, with ICs extracted from the first 10,000 members of the equilibrium climate distributions illustrated in figure 3.5, at given time instants. In all model runs, ρ varies according to equation 3.18 with a wave frequency, $f_i = 5LTU^{-1}$.

The KS results show that the ensembles converge to the same distributions, irrespective of the initial location for the IC ensemble. The IC uncertainty, encapsulated in the IC ensembles, does not appear to limit the long-term predictability of the climate distributions in the L63 model when subject to nonperiodic fluctuations in ρ. Moreover, the time scale for convergence is actually faster than that observed when ρ is constant (illustrated in figure 3.10). For constant values of ρ, the ensembles retain memory of the ICs after 30 LTUs and even after 40 LTUs in the Z variable. With nonperiodic fluctuations in ρ, the ensembles show no evidence of retaining memory of ICs after 30 LTUs and after 20 LTUs the values of D are only higher than the converged minimum values for IC ensembles 1 and 4 (most evident in the Z variable). The ensembles therefore appear to converge between 20 and 30 LTUs, 20 LTUs faster than when ρ is constant. The interpretation of this result is necessarily speculative given only four IC ensembles but it appears that for the model version considered here, the introduction of a time-dependent parameter fluctuation causes trajectories to spread about the model state space more rapidly than for a fixed value of ρ. This could be due to the changing nature of the underlying model attractor enabling the ensemble members to diverge more rapidly.

There is also a discernible discrepancy between IC ensembles in the first 15 LTUs of the simulation period. In figure 3.22, ensemble *IC 1* appears to converge more slowly than the other ensembles. For the first 15 LTUs, D is much larger for ensemble *IC 1* than it is for the other IC ensembles in the X and Y dimensions. In the Z dimension, ensemble *IC 4* also converges more slowly than ensemble *IC 2* and *IC 3*. Without further experimentation, it is difficult to generalise about the discrepancy between different IC ensembles at the early stages of the model simulation period but the difference in the model memory for different IC ensembles appears to be non-negligible.

The impact of a *time-dependent modulating attractor* on the model climate distributions, and the associated memory of ICs, is of interest in the analogy to the climate system which is subject to time-varying forcings. In chapters four and five, the notion of a *time-dependent modulating attractor* is explored further and the terminology used to describe this concept is refined. For the L63 model, further research with alternative perturbations to the parameter ρ might illuminate the dynamic features which control the evolution of the model climate distributions. In the next section, the work is extended to explore the changes to the model climate distributions when subject to trends in ρ.

3.8 Trends in ρ

An important uncertainty in climate change predictions is how internal climate variability will be affected under altered climate forcings. Cox and Stephenson (2007) assert that the fractional proportion of the total uncertainty in the future climate state attributable to uncertainty in the initial state of the climate system decreases smoothly over time. The underlying assumption is that the internal variability of the climate system is not dependent on the system forcings implying that internal climate variability will be the same under any forcing scenario. However, palaeoclimate evidence suggests that the internal variability of the climate system changes under altered forcing conditions (Overpeck and Webb (2000)). Using the L63 model to further extend the experiments conducted in this chapter, this section focuses on the internal variability of the model when subject to different trends in ρ, considered analogous to a climate forcing. The discussion relates the findings to the system *memory* (traceability of IC uncertainty). Understanding the relationship between internal climate variability, the forcing scenario and the memory of the system's ICs in a nonlinear system becomes highly relevant in guiding the design of climate model experiments to inform predictions relevant on adaptation time scales.

The experiments conducted in previous sections have focussed on the memory of the model for fixed, periodic and nonperiodic fluctuations in the forcing parameter ρ in the absence of any trends. The results show the impacts of fluctuations in ρ on the internal *climate* variability in the L63 model under fixed mean parameter conditions. The convergence of IC ensembles from different locations on the model attractor is shown to occur on a time scale of 40 to 50 LTUs for fixed values of ρ (section 3.4) and 20 to 30 LTUs for nonperiodic fluctuations in ρ (section 3.7.5). The extent to which IC ensembles from different initial locations on the L63 model attractor converge when subject to trends in the model parameters has not yet been considered. By introducing trends in the parameter ρ, the impact of transient parameter changes on the climate distributions of the L63 model is investigated.

3.8.1 L63 attractor for alternative values of ρ

In this section, the behaviour of the L63 model is investigated for a doubled value of ρ ($\rho = 56$) and a halved value of ρ ($\rho = 14$). As observed in section 3.5.2, increasing the parameter ρ leads to an increase in the ranges of the climate distributions for all model variables. Figure 3.23 shows the L63 attractor for a single model simulation when $\rho = 28$ (as in figure 3.1) and $\rho = 56$. Doubling the parameter ρ results in a shift of the attractor to increased values of Z and greater variability in the X and Y dimensions. The attractor retains a symmetry about the origin in the X and Y dimensions preserving the two-lobed structure. When ρ is decreased, the range of behaviour in all three dimensions decreases. For values of $\rho < \rho_H$ (associated with a Hopf bifurcation), the model is no longer chaotic over an infinite time scale. The regime structure of the L63 attractor is no longer observed and all trajectories propagate towards the model fixed points at $C^{\pm}$.

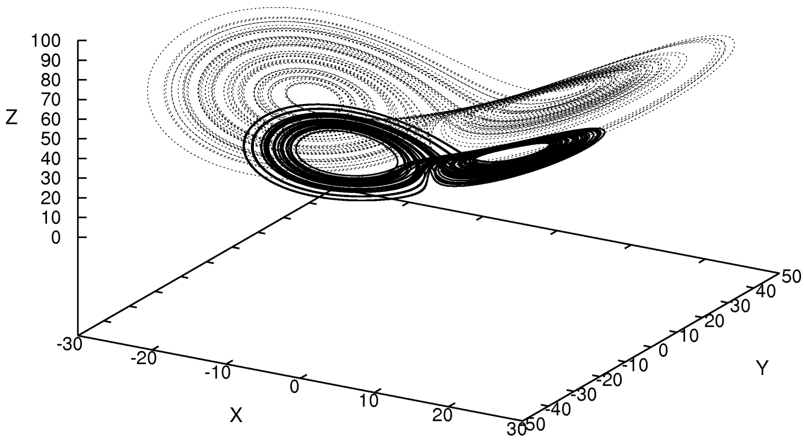

Figure 3.23: Single trajectory for a 50 LTU simulation of the L63 model with ICs $(X, Y, Z) = (1.0, 1.0, 25.0)$: $\rho = 28$ shown in solid line and $\rho = 56$ shown in dashed line.

Using the same approach adopted to determine the climate of the L63 model when $\rho = 28$, a 10,000 member IC ensemble is run (using ICs extracted from the first 10,000 members of the equilibrium climate distributions illustrated in figure 3.5) over a period of 1,000 LTUs for doubled and halved values of ρ. The final distribution of states for each variable are shown for $\rho = 56$ in figures 3.24(a) to 3.24(c) and for $\rho = 14$ in figures 3.24(d) to 3.24(f). When $\rho = 56$ the ensemble distributions appear unimodal and the secondary peaks found in the climate distributions when $\rho = 28$ are no longer apparent. The ranges in each dimension are increased, consistent with the attractor illustrated in figure 3.23. When $\rho = 14$ the ensemble distributions reveal that all trajectories have transitioned to the model fixed points located at $C^{\pm}$. In the X and Y distributions (figures 3.24(d) and 3.24(e)), the ensemble members are evenly split between the two fixed points. In fact, there are slightly more members located at C^{+} than C^{-} which highlights the sensitivity of the ensemble distributions to choice of ICs. In the Z dimension, all members are found at the fixed point located at $Z = 13$ $(\rho - 1)$.

3.8.2 System memory for fixed ρ

The IC ensemble distributions in figure 3.24 are used to represent the climate distributions of the L63 model when $\rho = 56$ and $\rho = 14$. The memory of the model is investigated for each value of ρ using the same four IC ensembles utilised in section 3.4 (displayed in figure 3.9). The four IC ensembles are run over a 200 LTU simulation period for the L63 model when $\rho = 56$ and $\rho = 14$. The KS test is used to compare the four ensemble distributions to the climate distributions at regular intervals: every 5 LTUs for the first 20 LTUs and every 10 LTUs for the remainder of the simulation period. The KS results for all three variables in each experiment are shown in figure 3.25.

Figures 3.25(a) to 3.25(c) show the KS comparisons when $\rho = 56$. The IC ensembles appear to converge to the model climate distributions over time but the convergence is slower than that observed in section 3.4 when $\rho = 28$. The memory of the model is therefore observed to

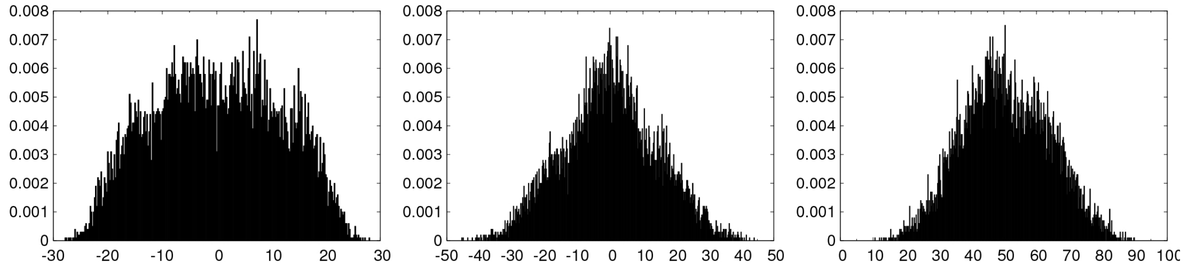

(a) X, $\rho = 56$ (b) Y, $\rho = 56$ (c) Z, $\rho = 56$

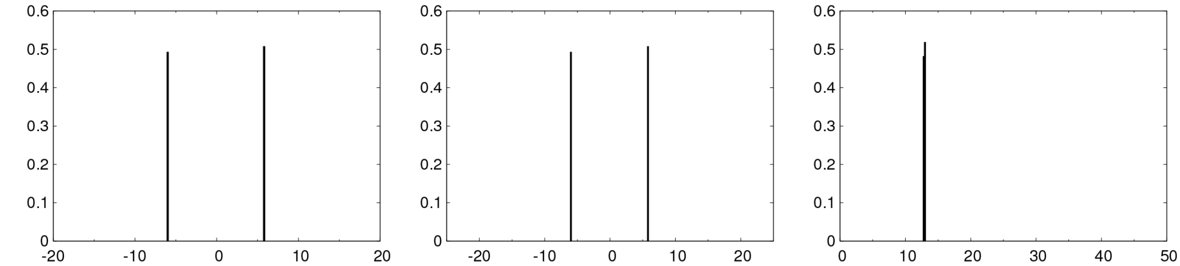

(d) X, $\rho = 14$ (e) Y, $\rho = 14$ (f) Z, $\rho = 14$

Figure 3.24: Normalised frequency distributions for the three L63 model variables when $\rho = 56$ (panels (a) to (c)) and when $\rho = 14$ (panels (d) to (f)), from a 10,000 member IC ensemble with ICs extracted from the first 10,000 members of the equilibrium climate distributions illustrated in figure 3.5. The distributions show the states of each ensemble member after a 1,000 LTU simulation period. In each plot, the x-axis is given by the panel title and the y-axis corresponds to the frequency of ensemble members per occupied bin; bin width = 0.2.

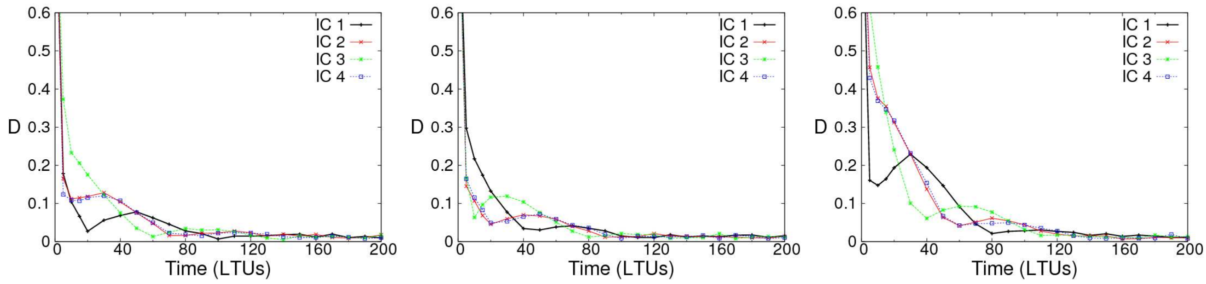

(a) X, $\rho = 56$ (b) Y, $\rho = 56$ (c) Z, $\rho = 56$

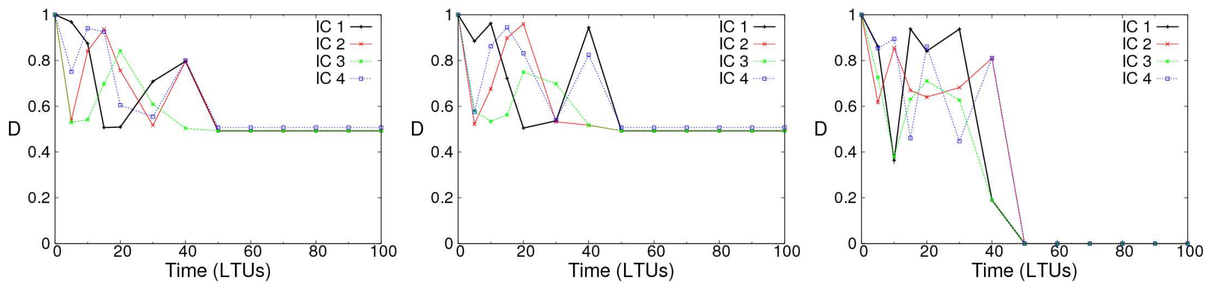

(d) X, $\rho = 14$ (e) Y, $\rho = 14$ (f) Z, $\rho = 14$

Figure 3.25: KS comparisons over time between the four different IC ensembles introduced in section 3.4 and the ensemble climate distributions given in figure 3.24, for each model variable, at given values of ρ.

increase when ρ is doubled. This is likely to occur because the range of state space occupied by the attractor at $\rho = 56$ is considerably larger than the range at $\rho = 28$ and therefore more time is required before trajectories can fully explore the attractor state space. There are some differences in the KS comparisons for each ensemble but the convergence times are fairly similar for all ensembles, occurring on a time scale of $t \approx 100$ LTUs. The convergence in the Z dimension is slower than in the X and Y dimensions and this is believed to be due to the asymmetry in the Z climate distribution as Z occupies only positive values. Ensembles 2 and 4 (labelled *IC 2* and *IC 4*) converge at broadly the same rate in all variables but this result is not observed when $\rho = 28$ indicating that convergence between individual ensembles is not consistent for different values of ρ.

Figures 3.25(d) to 3.25(f) reveal that the four IC ensembles fail to converge to the climate distributions in the X and Y dimensions when $\rho = 14$. Ensembles 1, 2 and 3 (labelled *IC 1*, *IC 2* and *IC 3*) converge to a minimum of $D = 0.49$ and ensemble 4 converges to $D = 0.51$. The memory of the ICs is therefore permanent as trajectories are unable to spread across the attractor state space before evolving to the fixed points. The ensembles converge in the Z dimension because there is only one fixed point in Z to which all trajectories evolve. All of the trajectories from the ensembles 1, 2 and 3 move to the fixed point at C^+ whilst the trajectories from ensemble 4 move to the fixed point at C^-. The plots reveal that memory of the individual ensembles is evident for 40 LTUs in each dimension before all ensemble members evolve to either of the two fixed points. This time scale is similar to that observed when $\rho = 28$.

3.8.3 System memory for increasing ρ

In this section and the next section, the memory of the model is investigated when subject to linear trends in ρ. Trends in ρ are introduced to examine the rates of convergence of ensembles originating in different locations of the model state space according to equation 3.19:

$$\rho(t) = \rho_0 + (\rho_f - \rho_0)\lambda^{-1}t \tag{3.19}$$

where ρ_0 is the initial value, ρ_f is the final value, t denotes time (LTU) and λ^{-1} is the gradient of the trend (LTU^{-1}). In the following experiments, when $\rho(t) = \rho_f$ the trend is stopped and ρ remains at ρ_f for the remainder of the simulation.

Initially, trends to the doubled value of ρ are investigated. The parameter values are therefore set to $\rho_0 = 28$ and $\rho_f = 56$. Three different gradients are explored to determine whether or not convergence of IC ensembles is a function of the trend/pathway of the parameter (forcing) in the L63 model. Figure 3.26 shows the different time-series' in ρ over a 100 LTU simulation period for positive trends with different values of λ.

The four IC ensembles introduced in section 3.4 and used in section 3.8.2 are utilised again in this section. The four ensembles are run with three different trends in ρ, shown in figure 3.26, and are compared to the evolution of a 10,000 member IC ensemble (with ICs extracted from

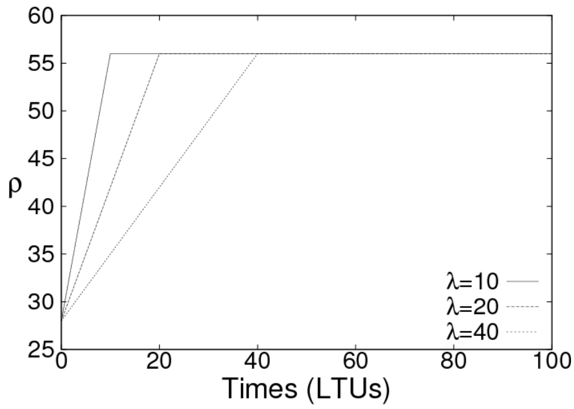

Figure 3.26: Time series' in ρ for different positive trends from $\rho_0 = 28$ to $\rho_f = 56$.

the first 10,000 members of the equilibrium climate distributions illustrated in figure 3.5) using the KS test at specific instants in the model simulations. The reference ensemble also evolves according to the time series' in ρ shown in figure 3.26. The KS comparisons for each variable and each trend in ρ are given in figure 3.27 for 200 LTU simulation periods.

The results in figure 3.27 show that the four IC ensembles from different locations on the initial attractor converge to the reference ensemble with ICs spread across the initial attractor. The results differ in detail for each of the four ensembles but there is no clear evidence that any of the ensembles converge more quickly than the others for all three variables under each trend in ρ. The key result from this experiment is that when the trend in ρ is more rapid, the convergence between the ensembles is slower. When $\lambda = 10$, the value of ρ increases from $\rho_0 = 28$ to $\rho_f = 56$ over a 10 LTU period and memory of the ICs is evident for at least 100 LTUs in the X and Y dimensions and possibly up to 150 LTUs in the Z dimension, as the value of D have still not converged towards a minimum. When $\lambda = 40$, the value of ρ increases from $\rho_0 = 28$ to $\rho_f = 56$ over 40 LTUs and memory of the ICs is evident for about 50 to 60 LTUs in the X and Y dimensions and 100 LTUs in the Z dimension. The attractor becomes larger in each dimension for higher values of ρ and the geometric properties of the attractor change more quickly when the trend in ρ has a high gradient (for low values of λ). Consequently, ensemble trajectories take longer to explore the attractor state space and converge towards the same distributions when the value of ρ increases rapidly.

In the analogy to climate prediction, the results suggest that it is worth considering the time scales at which uncertainty in the ICs is lost. In the L63 model, it has been shown that memory is dependent on the pathway of the parameter change; the more rapid the increase in ρ (to a new value ρ_f), the longer the memory in the model. The result implies that the memory of IC uncertainty in nonlinear systems might be forcing scenario dependent. It would be worth investigating this result to see if it is observed in more complex climate models.

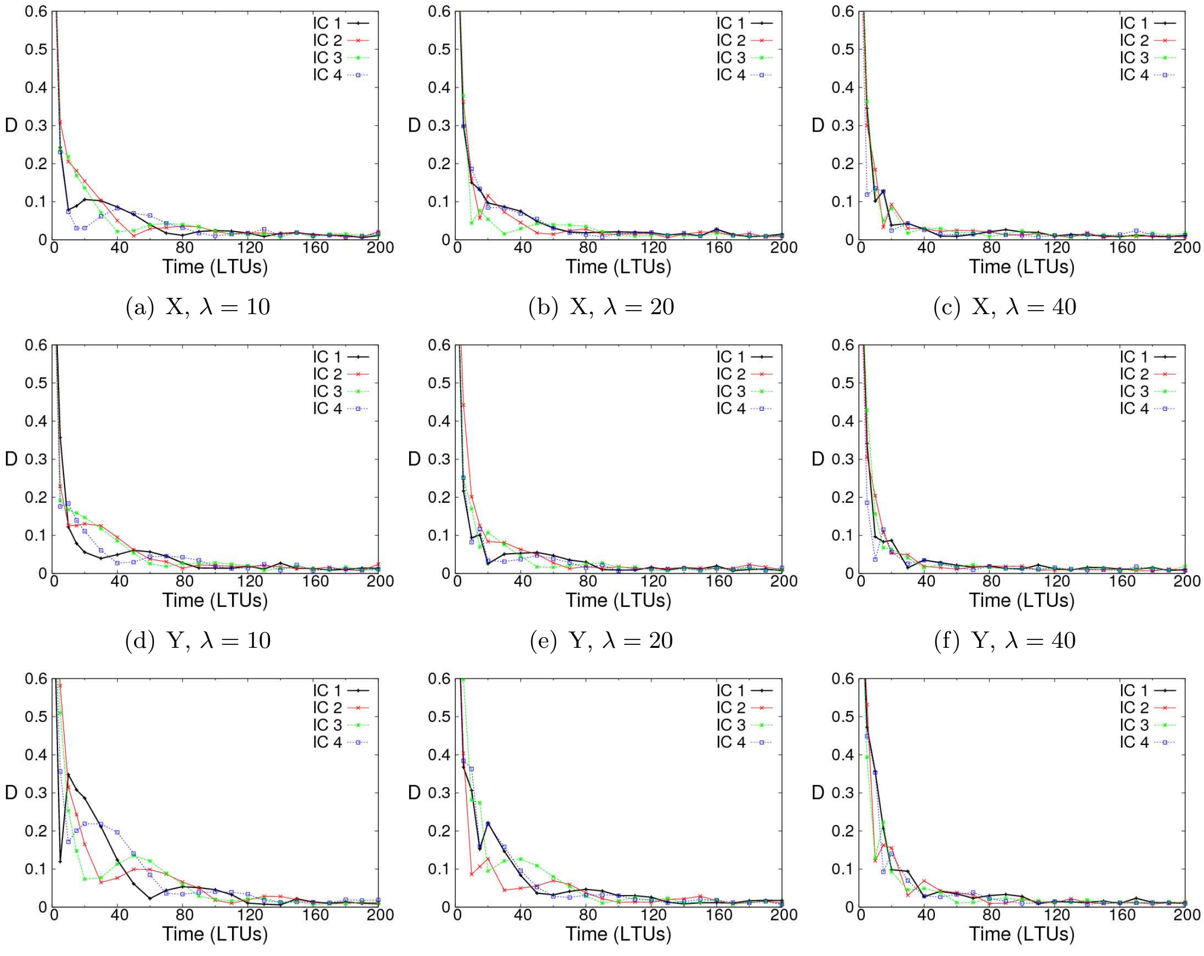

(a) X, $\lambda = 10$ (b) X, $\lambda = 20$ (c) X, $\lambda = 40$

(d) Y, $\lambda = 10$ (e) Y, $\lambda = 20$ (f) Y, $\lambda = 40$

(g) Z, $\lambda = 10$ (h) Z, $\lambda = 20$ (i) Z, $\lambda = 40$

Figure 3.27: KS comparisons over time between the four different IC ensembles introduced in section 3.4 and the IC ensemble with ICs extracted from the first 10,000 members of the equilibrium climate distributions illustrated in figure 3.5, for each model variable at given values of λ.

3.8.4 System memory for decreasing ρ

In the experiments conducted using the L63 model, the model simulations have been confined to chaotic regions of parameter space where the model is known to display transitive behaviour. In this section, the model is exposed to regions of parameter space that lead to non-chaotic behaviour. The same approach used in section 3.8.3 is adopted here for decreasing trends in ρ. The parameter values are set to $\rho_0 = 28$ and $\rho_f = 14$. Three negative gradients are explored to determine whether or not the convergence is a function of the trend/pathway in the parameter (forcing) when the model is moved into non-chaotic regions of parameter space. Figure 3.26 shows the different time-series' in ρ over a 100 LTU simulation period for negative trends with different values of λ.

The same four IC ensembles used throughout the analysis in this section are used once again and run with the three decreasing trends in ρ shown in figure 3.28. The distributions are compared

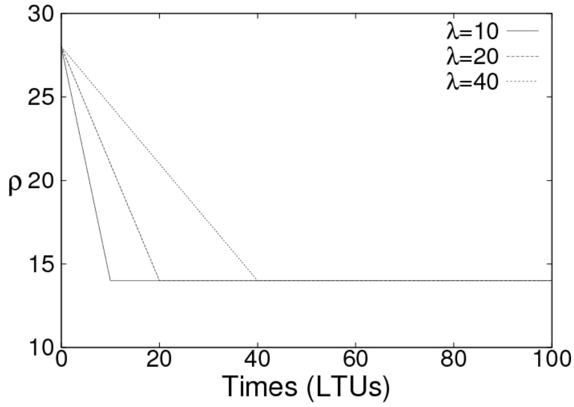

Figure 3.28: Time series' in ρ for different negative trends from $\rho_0 = 28$ to $\rho_f = 14$.

to the distributions resulting from the reference ensemble (used in the previous section), using the KS test. Figure 3.29 shows the KS results for negative trends in ρ. The KS comparisons reveal that the convergence between the four ensembles (with ICs from different locations on the initial attractor) to the reference ensemble (with ICs spread across the attractor) is dependent on the gradient of the trend. When $\lambda = -40$, convergence is observed in all variables. The decrease in the value of ρ is sufficiently slow to allow ensemble members to diverge across the attractor state space before they move to one of the fixed points ($C^{\pm}$) consistent with $\rho = 14$. When $\lambda = -20$, the ensembles converge in the Z dimension but only partially converge in the X and Y dimensions. At this rate of change in ρ, the ensemble trajectories are able to partially diverge but the resulting distributions of members between the two model fixed points are biased and therefore retain memory of the ICs. When $\lambda = -10$, the ensembles once again converge in the Z dimension but the convergence is slower than that observed when $\lambda = -20$ and $\lambda = -40$. In the X and Y dimensions, three of the ensembles converge to values of $D = 0.51$ whilst ensemble 4 converges to a value of $D = 0.05$. The result suggests that only ensemble members contained within ensemble 4 are able to diverge across the attractor state space before being attracted to one of the model's fixed points. This result is significant as it shows that not only is the trend in ρ important for the rate of convergence but also that when the model moves from a transitive region of parameter space to an intransitive region of parameter space, the exploration of the states consistent with the parameter conditions is dependent on the initial location of the IC ensemble.

The experimental results presented in this section are extended in the following chapter using a model which can be considered a closer analogy to the climate system. In chapter four, the dynamic behaviour of the Lorenz-84 model is investigated to elucidate the issue of moving between transitive and intransitive regions of parameter space which contain co-existing attractors.

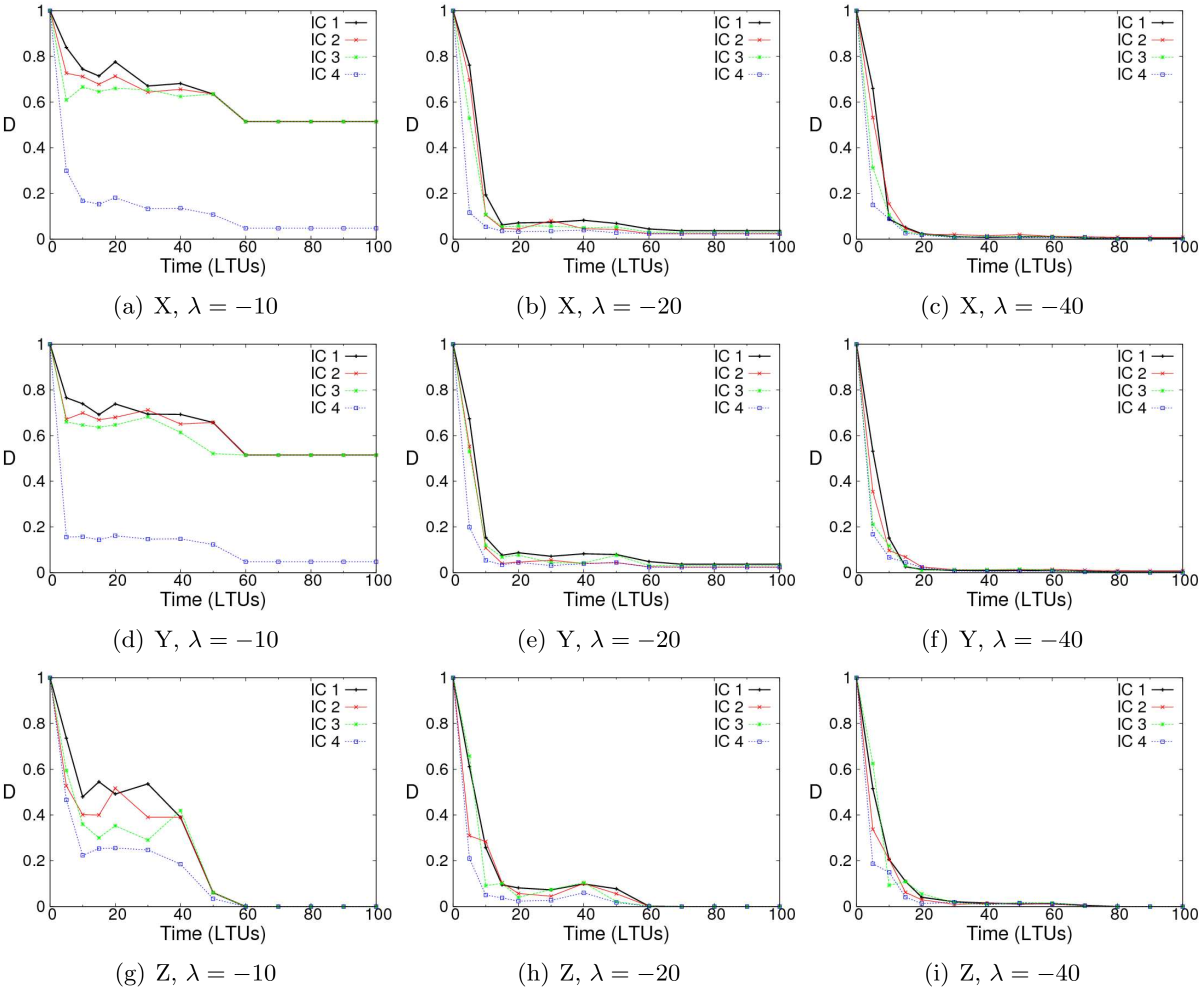

(a) X, $\lambda = -10$ (b) X, $\lambda = -20$ (c) X, $\lambda = -40$

(d) Y, $\lambda = -10$ (e) Y, $\lambda = -20$ (f) Y, $\lambda = -40$

(g) Z, $\lambda = -10$ (h) Z, $\lambda = -20$ (i) Z, $\lambda = -40$

Figure 3.29: KS comparisons over time between the four different IC ensembles introduced in section 3.4 and the IC ensemble with ICs extracted from the first 10,000 members of the equilibrium climate distributions illustrated in figure 3.5, for each model variable at given values of λ.

3.9 Discussion of L63 Results

3.9.1 Conceptual understanding of the climate system

Results from experiments conducted on simple models, such as the L63 model, are inevitably limited in their relevance to higher dimensional systems. Consequently, one cannot expect the results described in this chapter to generalise to higher-order climate models, let alone the real climate system. However, in exploring the rich dynamics of the L63 model, a better conceptual understanding of variability and change in complex nonlinear systems, such as the climate system, can emerge to inform the way climate model experiments are designed and to guide the interpretation of the output from complex climate models.

The motivation for the experiments conducted on the L63 model is to understand potential areas of uncertainty that may be poorly explored using conventional climate modelling methodologies. The emphasis is strongly on the implications of IC uncertainty and its impacts on system memory. In the following chapters, this theme continues to be addressed and the results of further experiments are described to illustrate potential limitations of existing climate model experimental designs.

In addressing the needs of the adaptation community, it is essential that *climate* and *climate change* are appropriately defined by the climate modelling community. The results presented in this chapter suggest that a statistical description of climate under climate change, which relies on the ergodic assumption, is insufficient to account for the potential effects of nonlinearities in the system's dynamics. In section 3.3.1, it is argued that the climate of the L63 model can be expressed as the distribution of possible system states consistent with the system's attractor. However, when the L63 model is subject to nonperiodic fluctuations in ρ, as shown in section 3.7, the ensemble distributions are observed to continuously change in accordance with the changing nature of the model's attractor. Both resonance and hysteresis effects are shown to be active factors in determining the climate model ensemble distributions. In refining the definition of climate to be suitable for climate change adaptation applications, climate ought to be defined as some future distribution of states consistent with the system's forcings, conditioned on the uncertainty in the initial state.

In section 3.7.4 the ergodic assumption is shown to fail when the model is subject to the nonperiodic parameter fluctuations. Whilst the model remains transitive, such that all possible model states can eventually be visited, the impact of varying the parameter ρ means that frequency distributions associated with a single trajectory do not represent the IC ensemble distributions at any instant in time. The results therefore show that for the non-autonomous L63 model, transitivity does not always imply ergodicity. If similar behaviour were to be observed in more complex climate models then the output of climate statistics based on single model realisations would be flawed.

The final section analysed the behaviour of the model when subject to trends in ρ. The results show that when the parameter values change, the dynamic behaviour of the model changes. The convergence time of IC ensembles from different locations on an attractor is slower when the parameter ρ increases and in the analogy to climate it might be the case that the memory of ICs becomes extended when the system's forcings are altered. Furthermore, experiments with the L63 model reveal that IC memory is permanent when moving from a chaotic region of parameter space to a non-chaotic region. Understanding the changes in dynamic behaviour of the climate system is therefore important in determining the relevance of different sources of prediction uncertainty.

3.9.2 Implications of resonance for climate model predictions

Resonant behaviour has previously been explored in the analysis of dynamical systems and is more commonly referred to as *stochastic* resonance for systems which undergo resonant-type behaviour as a function of the noise level (Gammaitoni et al. (1998)). The phenomena has been observed in the L63 model and related to the predictability of dynamic systems (Benzi et al. (1981), Crisanti et al. (1994), Sutera (1980)). Furthermore, the L63 model has been studied to understand the impact of stochastic resonance from variations in climate forcings on climatic change (Benzi et al. (1982), Tobias and Weiss (2000)). However, these studies have not explicitly acknowledged the potential effects of resonance on ensemble climate distributions. More recently, in relation to the potential of stochastic resonance to cause transitions between climatic regimes, Benzi (2010) stressed that fast variables should not be ignored in the study of long-term climate change.

The connection between the potential existence of resonant-type behaviour in the climate system and the way climate model experiments are designed to explore uncertainty is rarely made by scientists within the climate modelling community. Part of the reason for this may be attributable to the time scales on which the phenomena are deemed to be relevant. The focus of previous studies has predominantly been on the transitions between climate regimes on palaeoclimate time scales, which may be deemed largely irrelevant for decadal and multi-decadal climate predictions. However, in linking the design of climate model experiments to the information needs of decision makers, the potential of resonance to alter the shape of climate variable distributions ought to be evaluated. As argued by Stainforth et al. (2007a), and explored further in chapter 6, decisions regarding climate change adaptation are more often sensitive to the tails of climate distributions rather than shifts in the mean. Therefore, if there is a chance that the distribution of climate may be sensitive to resonance, at relevant spatial or temporal scales, then such a phenomenon ought to be accounted for in the exploration of uncertainty in climate model experiments. Furthermore, it is also important to distinguish between the impact of resonance and hysteresis on the climate. Even in the absence of any resonance effects, hysteresis can affect the climate distributions and such a possibility must also be recognised in the design of climate model experiments.

Given the results described in this chapter, particularly those illustrated in sections 3.6 and 3.7, it seems appropriate to hypothesize that if there is a mode of internal variability within the climate system that operates on a similar time scale to planetary scale forcings which impact the climate system, then the distribution of climate for certain variables at particular spatial scales may be highly sensitive to the phase and pathway of such forcings. Unfortunately, it is not possible to test such a hypothesis using the observational record, as there is only one observed trajectory for the evolution of the atmosphere-ocean system.

From a nonlinear dynamics perspective, the occurrence of erratic behaviour in the climate distributions of the L63 model, associated with temporal fluctuations in the parameter ρ, may indicate that the use of the term "attractor" is no longer suitable in the analysis of the system's behaviour. In dynamical systems research, other terms such as "stochastic", "pullback" and "random" have been used as a prefixes for the word attractor to extend the applicability of the term attractor into a non-autonomous context (Chekroun et al. (2010a), Chekroun et al. (2010b)). However, as a conceptual tool, the term attractor may still be valuable in understanding the implications of uncertain ICs and uncertain forcing scenarios on the ultimate evolution of the climate system.

3.9.3 Implications for climate model experimental design

Because of computational limitations, climate model simulations are rarely run with more than a handful of IC members. Therefore, when utilising climate model information to inform impacts models, the ergodic assumption is pervasive. The ergodic assumption has been shown to be invalid for the L63 model when subject to nonperiodic fluctuations in the parameter ρ, as outlined in section 3.7, and when ρ is forced into the non-chaotic region of parameter space, as shown in section 3.8. Therefore accurate estimates of the climate (as defined in section 3.3.1) of the L63 model cannot be achieved by single model realisations for certain parameter conditions. In making the case for considering large IC ensembles in climate model predictions, if the climate system exhibits hysteresis, then the absence of ergodicity suggests that the use of large IC ensembles is necessary to estimate the plausible distribution of climate states consistent with a particular climate forcing scenario.

In the transitive, chaotic regions of parameter space in the L63 model, convergence of IC ensembles is observed irrespective of the response to fluctuations in ρ. In extending the experiments conducted with L63 model to the Imperfect Model Scenario (IMS), any differences observed between IC ensemble distributions, after a period sufficient for convergence to occur, must be attributed to model error. By comparing the IC ensemble distributions which arise in the IMS to the IC ensemble distributions in the PMS, an estimate of the model discrepancy could be achieved. Such work would be a natural extension from the work presented in this chapter. For an ensemble of different models, assuming they are sufficiently independent from one another, comparisons between IC ensemble distributions from each model (under the same forcing scenario) at a given point in time and space could provide a valuable measure of model diversity and inform assessments of model reliability. Comparing single trajectory results only could not distinguish between errors caused by model inadequacy from anomalous features induced by internal climate variability.

In section 3.4, memory of ensemble IC location is shown to exist for a time scale of approximately 20 to 40 LTUs. However, the time scales in the L63 model are not directly comparable to those in the climate system so it is not possible to make any direct assertions regarding the time scale at which memory of ICs is lost in the climate system. However, understanding the time scale at which the initial state of the system is traceable will have important implications for decadal and longer time scale climate predictions. Using GCMs in a research mode to better estimate this time scale, by comparing the convergence rates of large IC model ensembles, is therefore potentially valuable in constraining the uncertainty in future climate projections. However, the climate system consists of many sub-systems operating on disparate time scales (e.g. ice sheets, oceans) which may blur any distinct time scale for memory of the initial state. In chapter five, the L84 model is coupled to the S61 model in order to address the issue of competing dynamic time scales.